AMERICAN SOCIETY FOR MICROBIOLOGY | mBio®

RESEARCH ARTICLE

PMRT1, a *Plasmodium*-Specific Parasite Plasma Membrane Transporter, Is Essential for Asexual and Sexual Blood Stage Development

Jan Stephan Wichers,[a,b,c] Paolo Mesén-Ramírez,[b] Gwendolin Fuchs,[a,b,c] Jing Yu-Strzelczyk,[d] Jan Stäcker,[b] Heidrun von Thien,[a,b] Arne Alder,[a,b,c] Isabelle Henshall,[e] Benjamin Liffner,[e] Georg Nagel,[d] Christian Löw,[a,f] Danny Wilson,[e,g] Tobias Spielmann,[b] Shiqiang Gao,[d] Tim-Wolf Gilberger,[a,b,c] Anna Bachmann,[a,b,c] Jan Strauss[a,b,c,f*]

[a]Centre for Structural Systems Biology, Hamburg, Germany
[b]Bernhard Nocht Institute for Tropical Medicine, Hamburg, Germany
[c]Biology Department, University of Hamburg, Hamburg, Germany
[d]Institute of Physiology, Department of Neurophysiology, Biocenter, University of Würzburg, Würzburg, Germany
[e]Research Centre for Infectious Diseases, School of Biological Sciences, University of Adelaide, Adelaide, Australia
[f]European Molecular Biology Laboratory, Hamburg Unit, Hamburg, Germany
[g]Burnet Institute, Melbourne, Victoria, Australia

Anna Bachmann and Jan Strauss contributed equally to this article.

ABSTRACT Membrane transport proteins perform crucial roles in cell physiology. The obligate intracellular parasite *Plasmodium falciparum*, an agent of human malaria, relies on membrane transport proteins for the uptake of nutrients from the host, disposal of metabolic waste, exchange of metabolites between organelles, and generation and maintenance of transmembrane electrochemical gradients for its growth and replication within human erythrocytes. Despite their importance for *Plasmodium* cellular physiology, the functional roles of a number of membrane transport proteins remain unclear, which is particularly true for orphan membrane transporters that have no or limited sequence homology to transporter proteins in other evolutionary lineages. Therefore, in the current study, we applied endogenous tagging, targeted gene disruption, conditional knockdown, and knockout approaches to investigate the subcellular localization and essentiality of six membrane transporters during intraerythrocytic development of *P. falciparum* parasites. They are localized at different subcellular structures—the food vacuole, the apicoplast, and the parasite plasma membrane—and four out of the six membrane transporters are essential during asexual development. Additionally, the plasma membrane resident transporter 1 (PMRT1; PF3D7_1135300), a unique *Plasmodium*-specific plasma membrane transporter, was shown to be essential for gametocytogenesis and functionally conserved within the genus *Plasmodium*. Overall, we reveal the importance of four orphan transporters to blood stage *P. falciparum* development, which have diverse intracellular localizations and putative functions.

IMPORTANCE *Plasmodium falciparum*-infected erythrocytes possess multiple compartments with designated membranes. Transporter proteins embedded in these membranes not only facilitate movement of nutrients, metabolites, and other molecules between these compartments, but also are common therapeutic targets and can confer antimalarial drug resistance. Orphan membrane transporters in *P. falciparum* without sequence homology to transporters in other evolutionary lineages and divergent from host transporters may constitute attractive targets for novel intervention approaches. Here, we localized six of these putative transporters at different subcellular compartments and probed their importance during asexual parasite growth by using reverse genetic approaches. In total, only two candidates turned out to be

Editor Louis H. Miller, NIAID/NIH

Address correspondence to Tim-Wolf Gilberger, gilberger@bnitm.de, or Jan Strauss, jstrauss@geomar.de.

*Present address: Jan Strauss, GEOMAR Helmholtz Centre for Ocean Research Kiel, Kiel, Germany.

The authors declare no conflict of interest.

Received 9 March 2022
Accepted 10 March 2022
Published 11 April 2022

dispensable for the parasite, highlighting four candidates as putative targets for therapeutic interventions. This study reveals the importance of several orphan transporters to blood stage *P. falciparum* development.

KEYWORDS *Plasmodium falciparum*, apicomplexan parasites, membrane proteins, membrane transport, reverse genetic analysis, subcellular localization, transporters

Malaria parasites inhabit diverse intracellular niches and need to import nutrients and export waste across both host cell and parasite membranes. Despite this, there are less than 150 putative membrane transporters encoded in the genome of *Plasmodium falciparum*, the most virulent malaria parasite, making up only 2.5% of all coding genes (*P. falciparum* 3D7 v3.2: 5,280 genes) (1–8), which is a reduced level compared to those of other unicellular organisms of similar genome size. The loss of redundant transporters is a typical feature of many intracellular parasites (9), and as a result, the proportion of transporters that are indispensable for parasite survival increases (2), some of which have been shown to be critical for the uptake of several antiplasmodial compounds and/or to be involved in drug resistance (10–23). Moreover, the parasite's intracellular lifestyle resulted in the evolution of additional specialized transporters without human homologues (1). During its intraerythrocytic development, the parasite relies on the uptake of nutrients, such as amino acids, pantothenate, or fatty acids, from its host erythrocyte as well as from the extracellular blood plasma (24–27). As *P. falciparum* resides in a parasitophorous vacuole (PV) in the host erythrocyte, nutrients acquired from the extracellular milieu must traverse multiple membranes: the erythrocyte plasma membrane, the parasitophorous vacuole membrane (PVM), the parasite plasma membrane (PPM), and eventually membranes of intracellular organelles, such as those of the apicoplast or mitochondria (24, 28–30). The unique requirements of malaria parasite survival have led to the evolution of a number of orphan transporters, whose localization or function cannot be predicted based on sequence homology to transporters in other organisms (4, 31). Despite the likely importance of uniquely adapted transporters to *P. falciparum* survival, subcellular localization, essentiality, function, and substrate specificity for most *P. falciparum* transporters have not been directly determined (2, 24, 29). The best functional evidence available for many *Plasmodium*-specific transporters comes from a recent knockout screen of these orphan transporters in the rodent malaria parasite *Plasmodium berghei* (31). However, whether observations for different transporters in the *P. berghei* model are directly transferrable to *P. falciparum* have yet to be examined. Therefore, in this study, we explore the localization and essentiality of four predicted orphan transporters that had been partially characterized in *P. berghei* and include two additional transporters with no experimental characterization available.

RESULTS

To date, the predicted "transportome" of *P. falciparum* consists of 117 putative transport systems (encoded by 144 genes) classified as channels ($n = 19$), carriers ($n = 69$), and pumps ($n = 29$) (2). The functions of the vast majority of transporter genes were inferred from sequence homology to model organisms; however, given their lack of homology, 39 gene products could not be associated with any function or subcellular localization and were categorized accordingly as orphan transporters (4). A subset of orphan transporters characterized in the *P. berghei* malaria model was selected for further characterization in *P. falciparum*. The four transporters selected were reported to be important at different stages of rodent malaria parasite growth with (i) *P. berghei* drug/metabolite transporter 2 (*Pf*DMT2; PF3D7_0716900) found to be essential for asexual blood stage development, (ii) *P. berghei* zinc transporter 1 (*Pf*ZIP1; PF3D7_0609100) was essential across transmission stages but not blood stages, where there was only a slight growth defect, (iii) *P. berghei* cation diffusion facilitator family protein (*Pf*CDF; PF3D7_0715900) knockout parasites had a defect during transmission stages but not during asexual stages, and (iv) *P. berghei*

major facilitator superfamily domain-containing protein (*Pf*MFS6; PF3D7_1440800) was found to be essential for parasite transmission from mosquitos to a new host, with a growth defect observed at asexual and gametocyte stages but not during mosquito stage parasite growth (31, 32). In order to confirm expression of these four, initially selected, transporters in *P. falciparum* asexual stages, we searched the list of "Genes coding for transport proteins" included in the Malaria Parasite Metabolic Pathways (MPMP) database (1, 33) for proteins with (i) transcriptome sequencing (RNA-seq) (34, 35) and (ii) proteomics evidence (36, 37) in asexual blood stages. During our initial searches of the MPMP database, but also including PlasmoDB (38) and the most recent *P. falciparum* 3D7 genome (v3.2) and annotations, we identified two additional putative transporters in *P. falciparum* (PF3D7_0523800 and PF3D7_1135300), whose *P. berghei* homologs were not targeted and functionally characterized by Kenthirapalan et al. (31) or investigated in any other experimental model. Given their obvious lack of sequence homology to transporter proteins in other evolutionary lineages and clear classification as orphan membrane transporters, both proteins were subsequently included in our characterization of *P. falciparum* orphan transporters and named "food vacuole resident transporter 1" (FVRT1; PF3D7_0523800) and "plasma membrane resident transporter 1" (PMRT1; PF3D7_1135300) based on their subcellular localization. AlphaFold-based structure predictions (39) and results from a structure homology search (40) of all six selected transporters are provided in Fig. S1 in the supplemental material.

Localization of putative *P. falciparum* transporters. To determine subcellular localization, we tagged the six putative transporters endogenously with green fluorescent protein (GFP) using the selection-linked integration (SLI) system (41) (Fig. 1A). Additionally, a glmS ribozyme sequence was included in the 3′ untranscribed region (3′ UTR), which enabled conditional gene knockdown upon addition of glucosamine (42). Correct integration of the plasmid into the respective genomic locus was verified by PCR and expression of the GFP-fusion protein was confirmed by Western blotting for each generated cell line (see Fig. S2A and B in the supplemental material).

All transgenic cell lines expressed the GFP-fusion protein, demonstrating that these transporters are expressed in asexual blood stage parasites (Fig. 1B to G; Fig. S2A). Expression levels were sufficient to allow determination of subcellular localization (Fig. 1B to G): (i) PF3D7_0523800-GFP localized to the food vacuole, (ii) *Pf*DMT2-GFP and *Pf*MFS6-GFP showed apicoplast localization, and (iii) *Pf*ZIP1-GFP and PF3D7_1135300-GFP showed PPM localization. However, *Pf*CDF-GFP showed an obscure staining pattern with a weak spot within the parasite cytosol in ring and trophozoite stage parasites, but multiple foci in schizont stages (Fig. 1D). To pinpoint this localization, an additional cell line with endogenously 3× hemagglutinin (3×HA)-tagged *Pf*CDF was generated, confirming the focal localization of *Pf*CDF in asexual stages (Fig. S2C).

Except for *Pf*CDF, the observed localizations of the other five transporters were confirmed by colocalization studies using appropriate episomally expressed marker proteins: P40PX-mCherry (43, 44) for the food vacuole, ACP-mCherry (45, 46) for the apicoplast, and Lyn-mCherry (41, 47) for PPM. The focal distribution of *Pf*CDF-GFP was colocalized with a rhoptry marker (ARO-mCherry [48, 49]) and a microneme marker (AMA1-mCherry [50, 51]), but *Pf*CDF-GFP did not colocalize with either marker (Fig. 1H). Additionally, for *Pf*ZIP and PF3D7_1135300, the PPM localization was further confirmed in free merozoites (Fig. S2D and *E*) and by confocal microscopy-based colocalization of PF3D7_1135300-GFP with the PPM marker Lyn-mCherry (Fig. S2F). Accordingly, as noted above, we named PF3D7_0523800 as "food vacuole resident transporter 1" (FVRT1) and PF3D7_1135300 as "plasma membrane resident transporter 1" (PMRT1).

Targeted gene disruption, conditional knockdown, and conditional knockout of putative transporters. In order to test whether the putative transporters are essential for *P. falciparum* during its intraerythrocytic cycle, we first tried to functionally inactivate them by targeted gene disruption (TGD) using the SLI system (41) (see Fig. S3A in the supplemental material). TGD cell lines were successfully obtained for *Pf*ZIP1 and *Pf*CDF (Fig. S3B and C). For *Pf*ZIP1-TGD, the correct integration of the plasmid into the genomic locus and absence of wild-type locus were verified by PCR, and subsequent

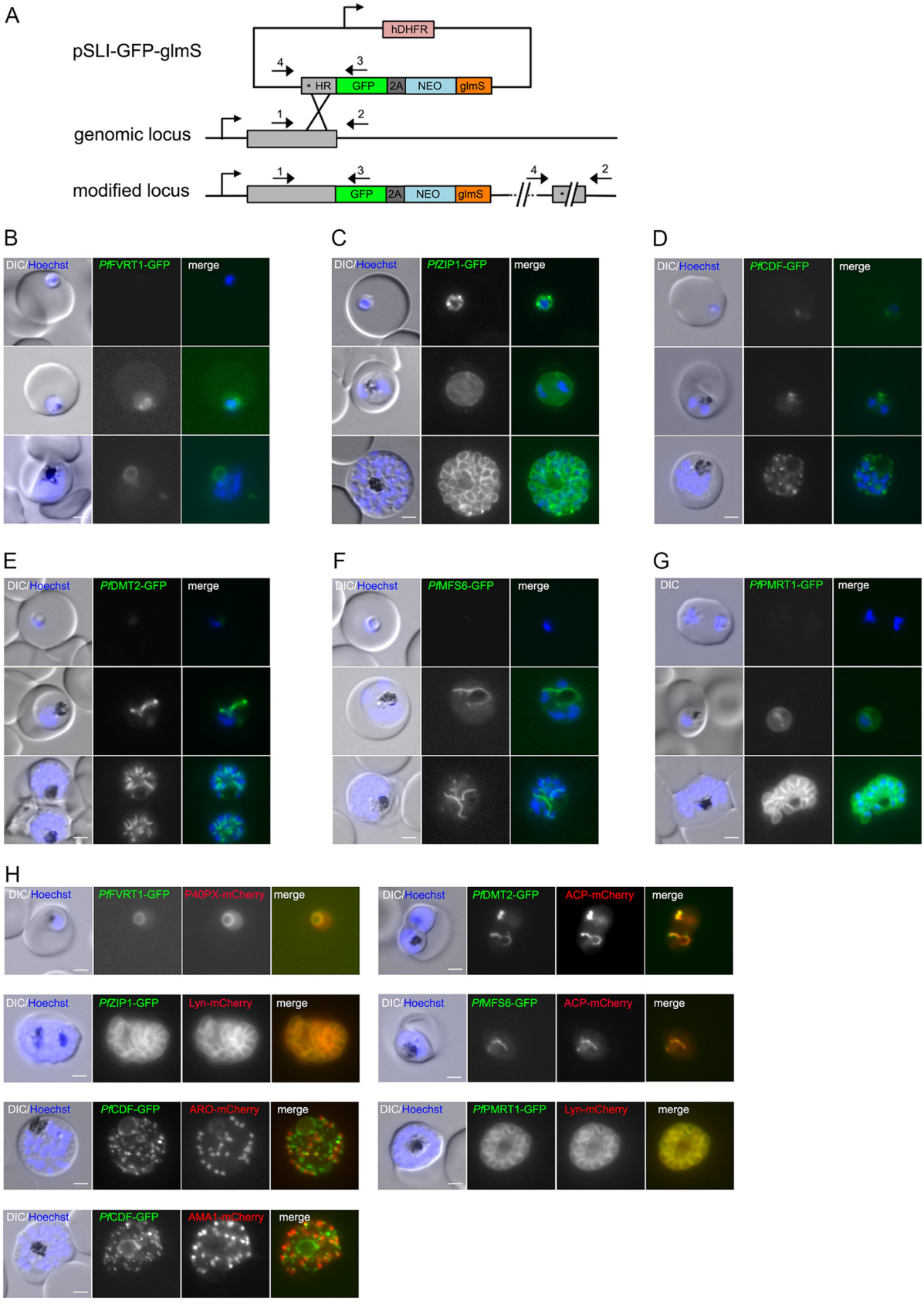

FIG 1 Subcellular localization of six putative *P. falciparum* transporters during asexual blood stage development. (A) Schematic representation of endogenous tagging strategy using the selection-linked integration system (SLI). Pink, human dihydrofolate dehydrogenase (hDHFR); gray,

(Continued on next page)

growth experiments revealed no growth defect compared to *P. falciparum* 3D7 wild-type parasites (Fig. S2B), suggesting its redundancy during asexual parasite proliferation. For *Pf*CDF-TGD, the correct integration of the plasmid into the genomic locus was also verified, but wild-type DNA was still detectable and remained even upon prolonged culturing under G418/WR selection and limited dilution cloning (Fig. S3C). In contrast, six (*Pf*PMRT1 and *Pf*DMT2) or eight (*Pf*FVRT1 and *Pf*MFS6) independent attempts to obtain TGD cell lines for the other four transporters with the respective plasmids failed, indicating that these genes have an indispensable role in blood stage parasite growth.

To probe the function of the putative transporters where we were unable to generate gene disruptions, we utilized the glmS ribozyme sequence. The corresponding sequence was integrated into the 3′ UTR of the targeted genes. This enabled the induction of conditional degradation of respective mRNAs upon addition of glucosamine (42) and the assessment of the phenotypic consequences. Upon addition of 2.5 mM glucosamine to young ring stage parasites, we found a 76.8% ± 3.7% (mean ± standard deviation [SD]) reduction in GFP fluorescence intensity in *Pf*DMT2-GFP parasites, a 72.7% ± 9.4% reduction in *Pf*MFS6-GFP, and a 77.7% ± 6.1% reduction in *Pf*PMRT1-GFP in schizonts of the same cycle (Fig. 2A to C; see Fig. S4A to C in the supplemental material). No measurable reduction in fluorescence intensity could be detected for *Pf*FVRT1-GFP or *Pf*CDF-GFP expressing parasite lines (Fig. S4D to F). The presence of the glmS cassette in both plasmids was confirmed by PCR (Fig. S4H). For parasite cell lines with a significant reduction in the expression of the endogenously tagged protein, proliferation was analyzed in the absence and presence of 2.5 mM glucosamine (Fig. 2D; Fig. S4G). While no significant effect on growth was observed for *Pf*MFS6, a growth reduction of 68.5% ± 2.1% over two cycles was observed upon knockdown of *Pf*DMT2. For *Pf*PMRT1, a minor growth delay was measurable, which resulted in a significantly reduced parasitemia at day 3 upon knockdown using 2.5 mM glucosamine (two-tailed Wilcoxon rank sum test, $W = 15$, $n_1 = 5$, $n_2 = 3$, $P = 0.03$), but was not significant when using 5 mM glucosamine (two-tailed Wilcoxon rank sum test, $W = 10$, $n_1 = 4$, $n_2 = 3$, $P = 0.16$) (Fig. 2E). Additionally, significantly fewer newly formed ring stage parasites were observed at 84 h postinvasion (hpi) (Fig. 2F), and multiple pairwise *post hoc* comparisons using the Conover-Iman rank sum test and Benjamini-Hochberg method to control the false discovery rates showed significant stepwise reductions of ring stage parasites after induction of glmS-based knockdown of *Pf*PMRT1 using both 2.5 mM glucosamine (adjusted $P = 0.0078$) and 5 mM glucosamine (adjusted $P = 0.0005$) in comparison to untreated control cell cultures.

To better characterize the minor growth phenotype of *Pf*PMRT1-GFP-glmS parasites that might be due to incomplete knockdown, we generated a conditional *Pf*PMRT1 knockout cell line (condΔPMRT1) using the dimerizable Cre (DiCre) system (52, 53). Again, using the SLI system (41), the endogenous *Pf*PMRT1 was disrupted upstream of the region encoding the N-terminal transmembrane domain, but at the same time introducing a recodonized second functional copy of *Pf*PMRT1 flanked by loxP sites in the genomic locus. This loxP-flanked allelic copy of *Pf*PMRT1 encodes an additional 3×HA tag, which can be conditionally excised upon addition of a rapamycin analog (rapalog) via the enzymatic activity of an episomally expressed DiCre (Fig. 3A). First, correct integration of the plasmid into the genomic locus was verified by PCR (Fig. 3B). Second, expression and localization of the recodonized HA-tagged protein at the PPM was verified by colocalization with the merozoite plasma membrane marker MSP1 (54) (Fig. 3C). Third, excision of the recodonized gene upon rapalog addition was confirmed at the genomic level by PCR (Fig. 3D) and at the protein level by Western blotting at 24 hpi and 48 hpi (Fig. 3E). To assess the effect of conditional *Pf*PMRT1 knockout on parasite proliferation, we determined growth of the transgenic parasite cell line

FIG 1 Legend (Continued)
homology region (HR); green, green fluorescent protein (GFP) tag; dark gray, T2A skip peptide; blue, neomycin resistance cassette; orange, glmS cassette. Stars indicate stop codons, and arrows depict primers (P1 to P4) used for the integration check PCR. (B to G) Localization of (B) *Pf*FVRT1-GFP-glmS, (C) *Pf*ZIP1-GFP-glmS, (D) *Pf*CDF-GFP-glmS, (E) *Pf*DMT2-GFP-glmS, (F) *Pf*MFS6-GFP-glmS, and (G) *Pf*PMRT1-GFP-glmS by live cell microscopy in ring, trophozoite, and schizont stage parasites. Nuclei were stained with Hoechst 33342. (H) Colocalization of the GFP-tagged putative transporters with marker proteins P40PX-mCherry (food vacuole), ACP-mCherry (apicoplast), Lyn-mCherry (parasite plasma membrane), ARO-mCherry (rhoptry), and AMA1-mCherry (microneme) as indicated. Nuclei were stained with Hoechst 33342. Scale bar, 2 μm.

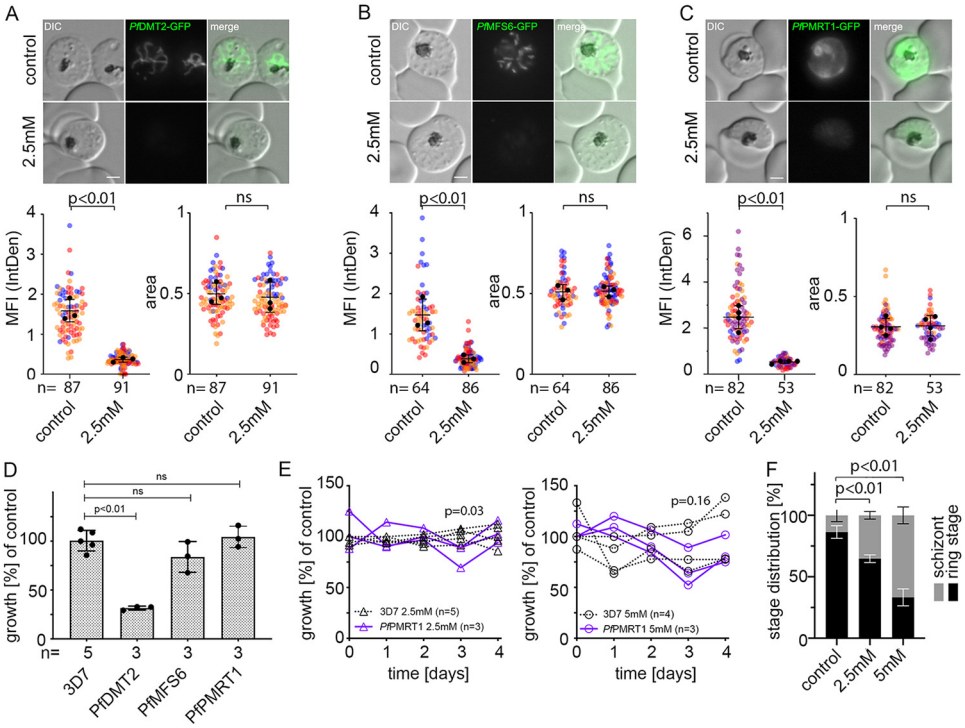

FIG 2 Conditional knockdown of putative transporter indicates the importance of *Pf*DMT2 and *Pf*PMRT1 for parasite fitness. (A to C) Live cell microscopy and quantification of knockdown by measuring mean fluorescence intensity (MFI) density and size (area) of (A) *Pf*DMT2-GFP-glmS (B) *Pf*MFS6-GFP-glmS, and (C) *Pf*PMRT1-GFP-glmS parasites 40 h after treatment without (control) or with 2.5 mM glucosamine. Scale bar, 2 μm. Statistics are displayed as mean ± SD from three (A and B) or four (C) independent experiments, and individual data points are color-coded by experiments according to SuperPlots guidelines (101). The *P* values displayed were determined by two-tailed unpaired *t* test. (D) Growth of parasites treated without (control) or with 2.5 mM glucosamine determined by flow cytometry is shown as relative parasitemia values after two cycles. Shown are means ± SD from three (*Pf*PMRT1-GFP-glmS, *Pf*DMT2-GFP-glmS, and *Pf*MFS6-GFP-glmS) and five (3D7 wild-type parasites) independent growth experiments. The *P* values displayed were determined by unpaired *t* test with Welch correction and Benjamin-Hochberg for multiple-testing correction. Individual growth curves are shown in Fig. S4G. (E) Growth of *Pf*PMRT1-glmS and 3D7 parasites after treatment with 2.5 mM (left panel) and 5 mM (right panel) glucosamine compared to untreated control parasites over 5 consecutive days. The *P* values displayed were determined for comparison between *Pf*PMRT1-glmS and 3D7 parasites at day 3 using the two-tailed Wilcoxon rank sum test. (F) Mean ± SD distribution of ring and schizont stage parasites in *Pf*PMRT1-glmS and 3D7 cell lines treated without (control) or with 2.5 mM or 5 mM glucosamine at 84 hpi (80 h postaddition of glucosamine) of three independent experiments. The *P* values displayed were determined using the Conover-Iman rank sum test and Benjamini-Hochberg method for multiple-testing correction after Kruskal-Wallis testing.

with and without rapalog over 5 days (Fig. 3F; see Fig. S5A in the supplemental material). In contrast to the glmS-based knockdown experiment, DiCre-based gene excision (induced by the addition of rapalog to young ring stages of condΔPMRT1 parasite cell cultures) abolished growth within the first replication cycle (Fig. 3F; Fig. S5A). The specificity of the observed growth phenotype was verified by gene complementation. To achieve this, we episomally expressed recodonized *Pf*PMRT1 with a TY1-epitope tag under either the constitutive *nmd3* or the weaker *sf3a2* promoter (55) in the condΔPMRT1 cell line (Fig. 3D and F; Fig. S5B and C). Correct localization of the TY1-tagged *Pf*PMRT1 at the PPM was verified by immunofluorescence assays (IFAs) (Fig. 3G). Notably, both complementations of the *Pf*PMRT1 knockout cell line (condΔPMRT1) with recodonized *Pf*PMRT1 under the control of either the constitutive *nmd3* or the weaker *sf3a2* promoter restored parasite growth (Fig. 3F; Fig. S5B and C). The level of growth restoration with low-level expression of recodonized *Pf*PMRT1 is in line with the results from glmS knockdown experiments, which showed that a reduction of about 75% in protein expression resulted only in a minor growth perturbation (Fig. 2C and D).

Loss of the PPM-localized *Pf*PMRT1 leads to an arrest of parasite development at the trophozoite stage and the formation of PPM-derived protrusions. To determine, which particular parasite stages are affected by the knockout of *Pf*PMRT1, we

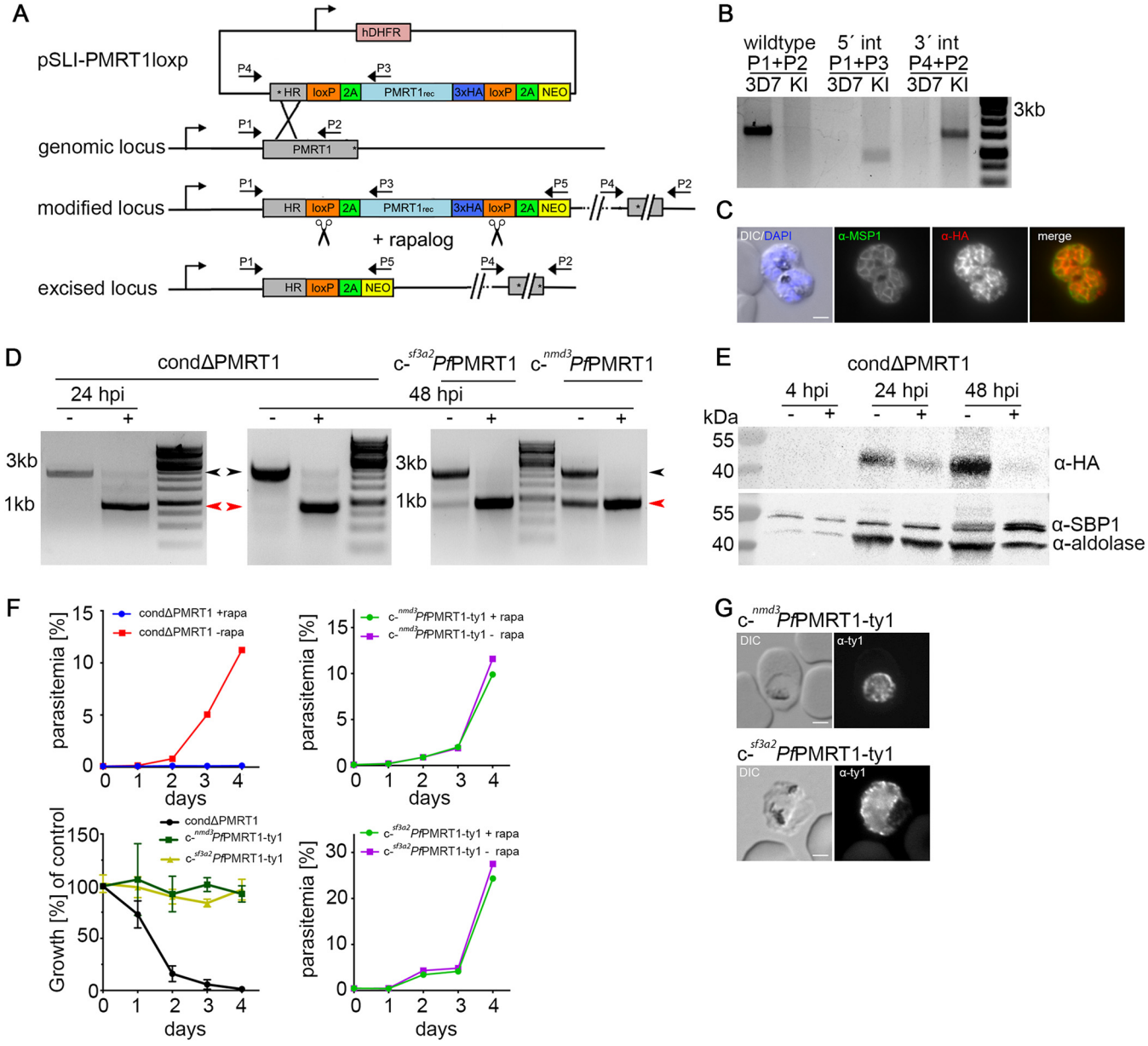

FIG 3 *Pf*PMRT1 is essential for asexual blood stage development. (A) Simplified schematic of DiCre-based conditional *Pf*PMRT1 knockout using selection-linked integration (SLI). Pink, human dihydrofolate dehydrogenase (hDHFR); gray, homology region (HR); green, T2A skip peptide; light blue, recodonized *Pf*PMRT1; dark blue, 3×HA tag; yellow, neomycin phosphotransferase resistance cassette; orange, loxP sequence. Scissors indicate DiCre-mediated excision sites upon addition of rapalog. Stars indicate stop codons, and arrows depict primers (P1 to P5) used for the integration check PCR and excision PCR. (B) Diagnostic PCR of unmodified wild-type and transgenic condΔPMRT1 knock-in (KI) cell line to check for genomic integration using Primer P1-P4 as indicated in panel A. (C) Immunofluorescence assay (IFA) of condΔPMRT1 late stage schizont parasites showing localization of *Pf*PMRT1-3×HA at the parasite plasma membrane (PPM) colocalizing with the merozoite surface protein 1 (MSP1). (D) Diagnostic PCR to verify the excision at the genomic level at 24 hpi/20 h post-rapalog addition for condΔPMRT1 and at 48 hpi for condΔPMRT1, c-^{nmd3}*Pf*PMRT1-ty1, and c-^{sf3a2}*Pf*PMRT1-ty1 parasites using primers P1 to P5 as indicated in panel A. Black arrowhead, original locus; red arrowhead, excised locus. (E) Western blot using anti-HA to verify knockout of *Pf*PMRT1 on the protein level 4, 24, and 48 hpi. The expected molecular weight of *Pf*PMRT1-3×HA is 53.3 kDa. Antibodies detecting aldolase and SBP1 were used as loading controls. (F) Growth curves of condΔPMRT1, c-^{nmd3}*Pf*PMRT1-ty1, and c-^{sf3a2}*Pf*PMRT1-ty1 parasites ± rapalog monitored over 5 days by flow cytometry. One representative growth curve is depicted (replicates in Fig. S5). The summary is shown as relative parasitemia values, which were obtained by dividing the parasitemia of rapalog-treated cultures by the parasitemia of the corresponding untreated ones. Shown are means ± SD from three (condΔPMRT1 and c-^{nmd3}*Pf*PMRT1-ty1) or four (c-^{sf3a2}*Pf*PMRT1-ty1) independent growth experiments. (G) IFA of condΔPMRT1 complemented with C-terminal TY1-tagged *Pf*PMRT1 constructs expressed under either the constitutive *nmd3* or the weak *sf3a2* promoter to verify PPM localization. Scale bar, 2 μm.

added rapalog to tightly synchronized parasites at different time points (4, 20, and 32 hpi) (Fig. 4A) and monitored parasite growth by flow cytometry. Additionally, we quantified growth perturbation by microscopy of Giemsa smears at 4, 20, 24, 32, 40, 48, 72, and 96 hpi (Fig. 4B; see Fig. S6A and B in the supplemental material). When rapalog

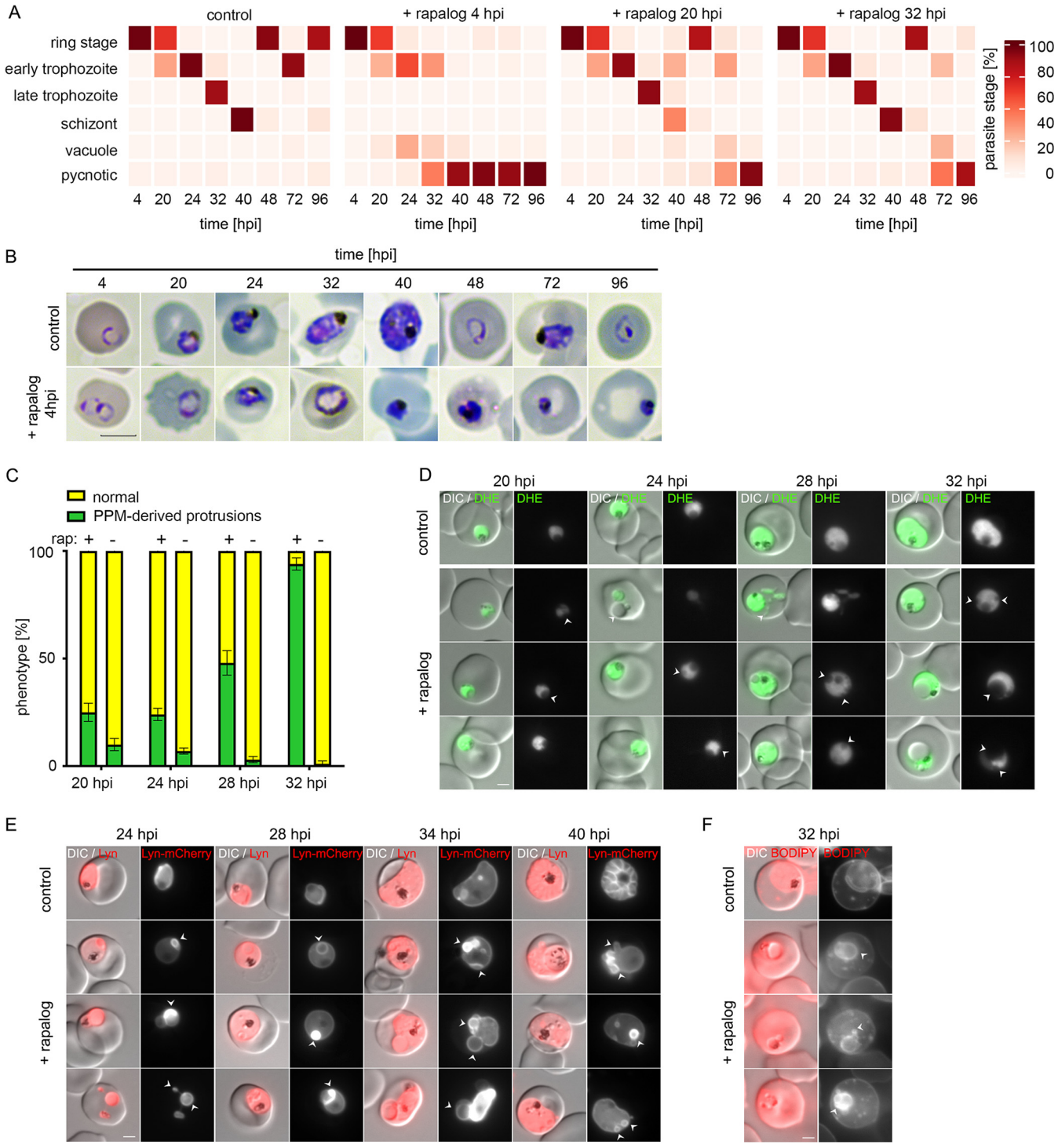

FIG 4 Knockout of *Pf*PMRT1 results in accumulation of PPM-derived protrusions and growth arrest at the trophozoite stage. (A) Parasite stage distribution in Giemsa smears displayed as a heat map showing the percentage of parasite stages for tightly synchronized (±2 h) 3D7 control and condΔPMRT1 (rapalog treated at 4 hpi, 20 hpi, or 32 hpi) parasite cultures over two consecutive cycles. A second replicate is shown in Fig. S6A. (B) Giemsa smears of the control and at 4 hpi rapalog-treated condΔPMRT1 parasites over two cycles. Scale bar, 5 μm. (C) Live cell microscopy of 4-h window synchronized 3D7 control and condΔPMRT1 parasites ± rapalog stained with dihydroethidium (DHE) at 20 to 32 hpi. (D) Quantification of parasites displaying protrusions (green) for 4-h window synchronized 3D7 control and rapalog-treated condΔPMRT1 parasites. Shown are percentages of normal parasites versus parasites displaying protrusions as means ± SD from three independent experiments. (E) Live cell microscopy of 8-h window synchronized 3D7 control and rapalog-treated condΔPMRT1 parasites, episomally expressing the PPM marker Lyn-mCherry at 24 to 40 hpi. (F) Live cell microscopy of 3D7 control and condΔPMRT1 parasites ± rapalog stained with BODIPY TR C5 ceramide at 32 hpi. Scale bar, 2 μm.

was added at 4 hpi, parasite development progressed through the ring and early trophozoite stages up to 24 hpi with no visible abnormality. Afterwards, parasites with deformed and enlarged protrusions started to appear, and further development stalled. At 32 hpi, almost all parasites had developed to late trophozoites/early schizonts in the control, whereas these stages were completely absent in *Pf*PMRT1-deficient parasites. Over 50% of the parasites were pycnotic or possessed large protrusions; the remaining parasites stayed arrested at the trophozoite stage. Quantification of the percentage of parasites with protrusions between 20 hpi and 32 hpi revealed 94.8% ± 4.0% protrusion-positive parasites (Fig. 4C). The activation of gene excision at later time points by adding rapalog at 20 hpi or 32 hpi resulted in no or minor growth perturbation in the first cycle with successful reinvasion, but again led to parasites arresting at the trophozoite stage in the second cycle with an accumulation of protrusions (Fig. 4A; Fig. S6A and B).

In order to gain further insights into the morphological changes in *Pf*PMRT1-deficient parasites, we incubated these parasites with dihydroethidium (DHE) to visualize the parasite cytosol (44). We observed an absence of staining within the protrusions, suggesting they are not filled with parasite cytosol (Fig. 4D). Next, we transfected the condΔPMRT1 cell line with a plasmid encoding the PPM marker Lyn-mCherry (41) and observed Lyn-mCherry-positive protrusions upon knockout of *Pf*PMRT1 starting to become visible at 24 hpi, indicating that the protrusions originate from the PPM (Fig. 4E). In line with this, protrusion membranes were also stainable with BODIPY TR C5 ceramide in condΔPMRT1 parasites at 32 hpi (Fig. 4F).

Depletion of *Pf*PMRT1 results in an early arrest of gametocyte development. RNA-seq data suggest *Pf*PMRT1 is also expressed during other developmental stages, such as gametocytes (56, 57). Therefore, we assessed expression of *Pf*PMRT1-GFP during gametocytogenesis by reengineering *Pf*PMRT1-GFP-glmS in the inducible gametocyte producer (iGP) 3D7-iGP (58) parasite line, which allows the robust induction of sexual commitment by conditional expression of gametocyte development 1 protein (GDV1) upon addition of shield-1 (58) (see Fig. S7A in the supplemental material). We show that *Pf*PMRT1 is indeed expressed during all stages of gametocytogenesis and again localizes to the PPM, colocalizing with the PPM marker Lyn-mCherry (41) (Fig. 5A and B). Conditional knockdown of *Pf*PMRT1 via the glmS ribozyme system (Fig. S7B) resulted in a reduction in *Pf*PMRT1-GFP fluorescence intensity of 79.4% ± 9.2% at 7 days postinduction (dpi) or 75.5% ± 23.2% at 10 dpi, without an effect on gametocyte development (Fig. S7C to F). In order to exclude that a role of *Pf*PMRT1 in gametocytogenesis is covered up by only a partial knockdown, resulting in low levels of expressed protein, and to determine if *Pf*PMRT1 is essential for gametocytogenesis, we episomally expressed GDV1-GFP-DD in the condΔPMRT1 parasite line, enabling conditional induction of sexual commitment upon addition of shield-1 in these parasites (59). Conditional knockout of *Pf*PMRT1 in these transgenic parasites at day 3 post-gametocyte induction resulted in pycnotic parasites from day 5 onwards, while excision of *Pf*PMRT1 at day 5 postinduction had no effect on gametocyte development (Fig. 5C and D). Excision of the recodonized gene upon rapalog addition was confirmed at a genomic level by PCR for both conditions (Fig. 5E). Quantification of parasite stages at day 10 postinduction of GDV1 expression revealed 77.9% ± 7.7% gametocytes and 22.1% ± 7.7% pycnotic parasites in the control, while 100% of parasites were already pycnotic in the cultures, with induced knockout by addition of rapalog at day 3 post-gametocyte induction by GDV1 expression (Fig. 5F). This data indicates that *Pf*PMRT1 is important for early gametocyte development.

PMRT1 is unique to the genus *Plasmodium*, and interspecies complementation assays showed partial functional conservation. *Pf*PMRT1 shows a lack of sequence similarities to known or putative transporters and/or conserved domains shared with known transporter families (2, 5). Our phylogenetic analysis revealed that homologs of *Pf*PMRT1 are present across *Plasmodium* species with amino acid sequence identities of about 90% in the subgenus *Laverania*, but about 50% outside *Laverania* (Fig. 6A). However, prediction of the protein structure using AlphaFold (39) indicates two

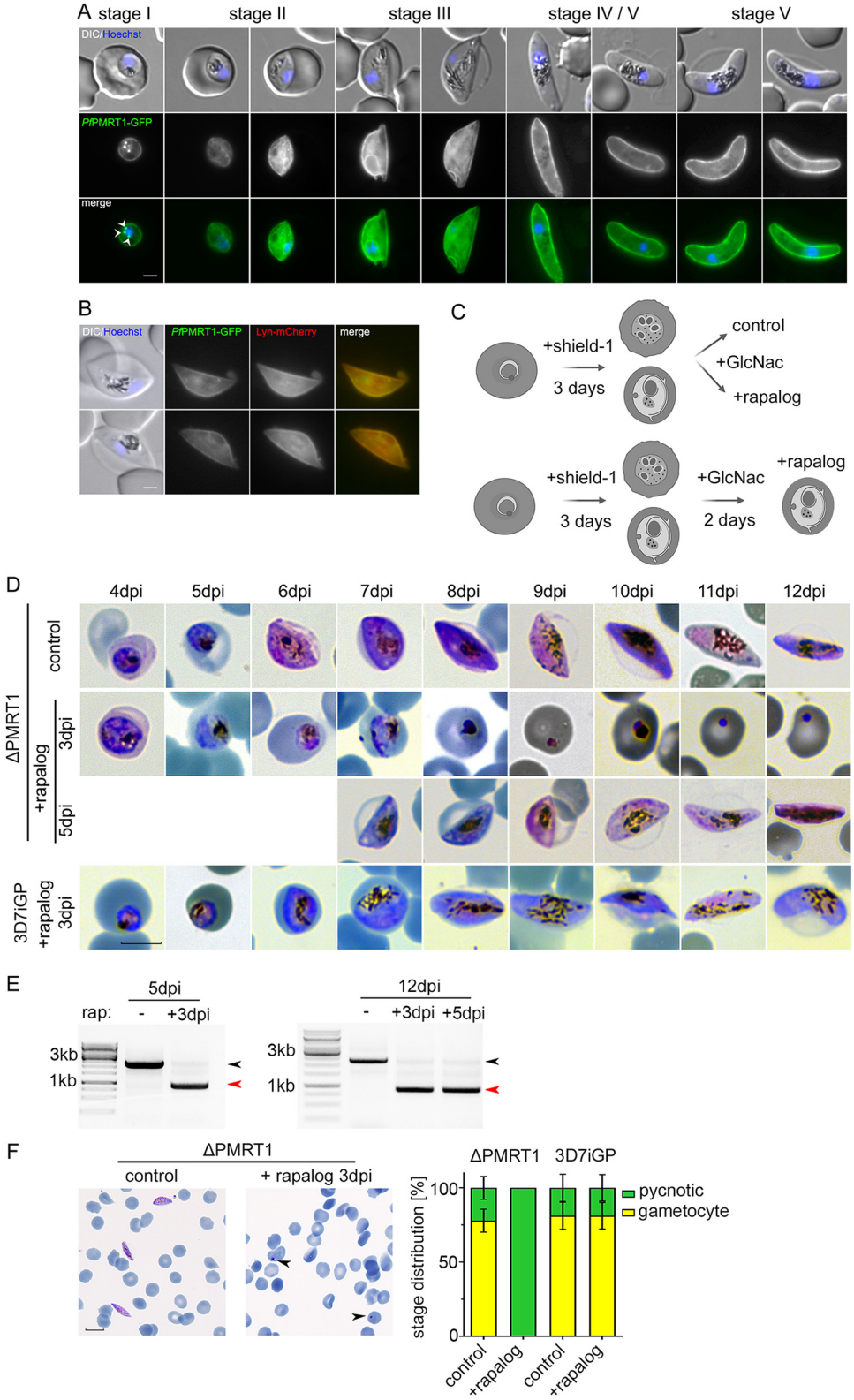

FIG 5 *Pf*PMRT1 is essential for early gametocyte development. (A) Live cell microscopy of 3D7-iGP-*Pf*PMRT1-GFP parasites across the complete gametocyte development. White arrowheads indicate remaining GDV1-GFP signal observed in close proximity to the Hoechst signal, as previously reported (59, 94, 102, 103). (B) Live cell microscopy of *Pf*PMRT1-GFP parasites expressing the PPM marker Lyn-mCherry. Nuclei were stained with Hoechst 33342. Scale bar, 2 μm. (C) Experimental setup of gametocyte induction upon GDV1-GFP-DD expression (+shield-1) and conditional *Pf*PMRT1 knockout (+rapalog) and elimination of asexual blood stage

(Continued on next page)

bundles of four transmembrane helices with reasonable similarity of the C-terminal bundle to the photosynthetic reaction center Maquette-3 protein (60) (root mean square deviation [RMSD] of 3.12) (Fig. 6B; Fig. S1B). In order to test for functional conservation, we expressed the *Pf*PMRT1 homologs of *Plasmodium vivax* (PVP01_0936100) and *Plasmodium knowlesi* (PKNH_0933400) episomally as C-terminal Ty-1 fusion proteins under the *nmd3* promoter in the condΔPMRT1 parasites. Both fusion proteins are expressed. They were again localized at the PPM, as shown by IFA (Fig. 6C; see Fig. S8 in the supplemental material), and, importantly, were able to partially restore growth after two cycles to 64.8% ± 9.8% and 65.1% ± 7.4% compared to condΔPMRT1 parasites (Fig. 6D; Fig. S8). Excision of the recodonized endogenous *Pfpmrt1* gene upon rapalog addition was confirmed at a genomic level by PCR (Fig. 6E). These data indicate that PMRT1 is functionally conserved within the genus *Plasmodium*.

DISCUSSION

In this article, we have functionally described four so-called "orphan transporters" (31) in *P. falciparum*, which were partially characterized in *P. berghei*, and include two additional so-far-uncharacterized proteins with a transporter sequence signature.

We localized *Pf*FVRT1-GFP—annotated on PlasmoDB (38) as a putative divalent metal transporter—at the food vacuole of the parasite, which is in line with a previously predicted food vacuole association (1) and its reported homology (1, 61) to the conserved eukaryotic endosomal/lysosomal natural resistance-associated macrophage protein (NRAMP) transporter (62) in our structure similarity search. Repeated attempts to generate a TGD cell line failed, indicating an important role of this transporter during asexual blood stage development, which is in agreement with data from a *P. falciparum* genome-wide essentiality screen (63).

In concordance with recently published data identifying *Pb*DMT2 and *Pb*MFS6 as leaderless apicoplast transporters (32), we localized GFP-fusion proteins of *Pf*DMT2 and *Pf*MFS6 at the apicoplast. Successful knockdown of *Pf*DMT2 resulted in a growth defect in the second cycle after induction, resembling the described delayed death phenotype of other apicoplast genes that were functionally inactivated (32, 64–66). This suggests an essential role of *Pf*DMT2 in apicoplast physiology, as observed by Sayers et al. (32) for the rodent malaria organism *P. berghei*. This is further supported by our failed attempts to disrupt this gene using the SLI system.

We also failed to disrupt the *Pf*MFS6 locus, which is in agreement with the gene knockout studies in *P. berghei* that led to a markedly decreased multiplication rate (31, 32, 67). Nevertheless, glmS-based knockdown, although comparable to *Pf*DMT2-GFP knockdown (72.7% versus 76.8% reduction in GFP fluorescence, respectively) had no effect on parasite proliferation in our study. This might indicate that these reduced levels of *Pf*MFS6, in contrast to reduced levels of *Pf*DMT2, are sufficient for normal asexual replication *in vitro*.

Another candidate, *Pf*CDF, annotated as a putative cation diffusion facilitator family protein, showed multiple cytosolic foci within the parasite with no colocalization with apical organelle markers. The homologue in *Toxoplasma gondii*, *Tg*ZnT (TgGT1_251630), shows a similar cellular distribution (68). It has recently been shown to transport Zn^{2+}, to localize to vesicles at the plant-like vacuole in extracellular tachyzoites, and to be present

FIG 5 Legend (Continued)
parasites (+GlcNac). (D) Gametocyte development over 12 days of condΔPMRT1/GDV1-GFP-DD or 3D7-iGP parasites without (control) or with rapalog addition at day 3 (3 dpi) or day 5 (5 dpi) after induction of sexual commitment by conditional expression of GDV1-GFP upon addition of shield-1. Scale bar, 5 μm. (E) Diagnostic PCR to verify the excision at the genomic level at 5 dpi and 12 dpi. Black arrowhead, original locus; red arrowhead, excised locus. (F) Representative Giemsa smears and quantification of parasite stage distribution at day 10 postinduction for parasites treated without (control) or with rapalog at day 3 postinduction. For each condition, the distributions of parasitemia and parasite stages in erythrocytes of three independent experiments were determined and are displayed as percentage (ΔPMRT1, $n_{control}$ = 3,370, 2,304, and 2,759, and $n_{rapalog}$ = 3,010, 1,830, and 2,387; 3D7-iGP, $n_{control}$ = 4,985, 4,685, and 5,206, and $n_{rapalog}$ = 4,930, 4,332, and 5,384). Nuclei were stained with Hoechst 33342. Scale bar, 10 μm.

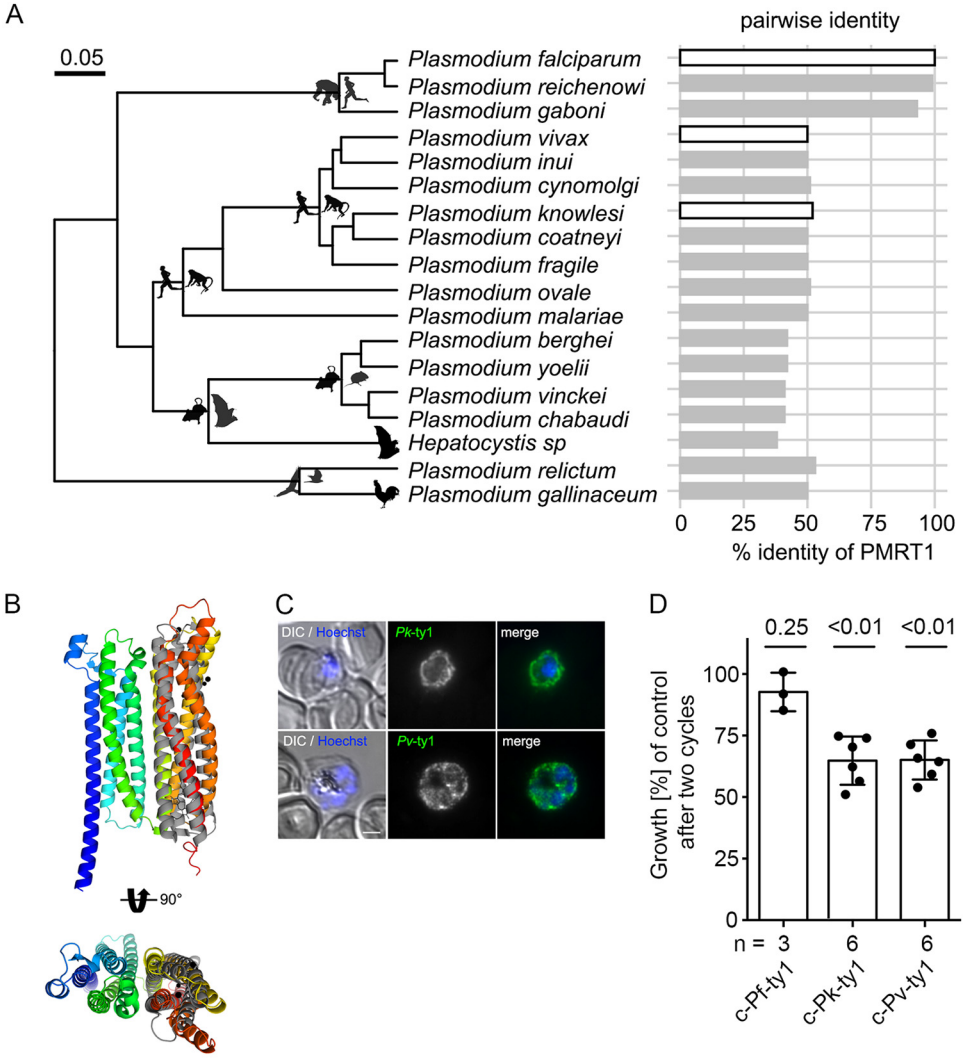

FIG 6 PMRT1 is a genus-specific transporter with conserved function. (A) Phylogenetic tree of haemosporidian parasites (including information previously presented in 95) containing PMRT1 homologous sequences associated with data on pairwise amino acid sequence identity to *Pf*PMRT1. The phylogeny is derived from Bayesian inference using BEAST with a fully partitioned amino acid data set and log-normal relaxed molecular clock (95). Silhouettes depict representatives of the vertebrate hosts for each lineage, and white bars indicate pairwise identities of PMRT1 homologs used for subsequent complementation assays. (B) Structural alignment of predicted *Pf*PMRT1 structure with Maquette-3 protein (PDB accession no. 5vjt) (60). Both structures have a root mean square deviation (RMSD) over the aligned α-carbon position of 3.12 over 184 residues calculated in PyMol. (C) IFA of c-^{nmd3}*Pk*-ty1 and c-^{nmd3}*Pv*-ty1 parasites to verify correct localization of the expressed complementation fusion proteins at the parasite plasma membrane. Nuclei were stained with Hoechst 33342. Scale bar, 2 μm. (D) Growth of condΔPMRT1 parasites complemented with *Pf*PMRT1 homologs from *P. vivax* (PVP01_0936100) and *P. knowlesi* (PKNH_0933400). Shown are relative parasitemia values, which were obtained by dividing the parasitemia of rapalog-treated cultures by the parasitemia of the corresponding untreated controls together with means ± SD from three c-^{nmd3}*Pf*-ty1 (≙c-^{nmd3}*Pf*PMRT1-ty1) (Fig. 3D; Fig. S5B) and six (c-^{nmd3}*Pk*-ty1 and c-^{nmd3}*Pv*-ty1) independent growth experiments. A one-sample *t* test was performed. (E) Diagnostic PCR to verify the excision of *Pf*PMRT1 at the genomic level at 48 hpi for c-^{nmd3}*Pf*-ty1, c-^{nmd3}*Pk*-ty1, and c-^{nmd3}*Pv*-ty1 parasites. Black arrowhead, original locus; red arrowhead, excised locus.

at dispersed vesicles throughout the cytoplasm of intracellular tachyzoites (68). The essentiality of *Pf*CDF for *in vitro* blood stage growth is debatable. We were not able to generate a clonal wild-type-free TGD cell line, although correct integration of the plasmid into the genomic locus could be verified (Fig. S3C). This points toward its dispensability for *in vitro* blood stage growth, which is supported by (i) its high (1.0) mutagenesis index score in a *P. falciparum* genome-wide mutagenesis screen (63) and (ii) gene deletion experiments in rodent malaria species showing that CDF proteins are nonessential for *in vivo* blood stage development in *Plasmodium yoelii* (69) and *P. berghei* (31, 67).

Finally, two putative transporters, *Pf*ZIP1 and *Pf*PMRT1, localized to the PPM. We show that *Pf*ZIP1 is nonessential for *P. falciparum in vitro* blood stage development, in line with a high (0.7) mutagenesis index score in a *P. falciparum* genome-wide mutagenesis screen (63). However, this is in contrast to the reported strong fitness loss in *P. berghei* (67) knockout mutants and failed knockout attempts in *P. yoelli* and *P. berghei in vivo* mouse models (32, 69). These observations may reflect differences between *Plasmodium* species or differing requirements for *in vitro* and *in vivo* growth conditions.

*Pf*PMRT1 is annotated as a conserved *Plasmodium* membrane protein with unknown function. It has been described as a protein showing structural characteristics of a transporter, without sharing sequence similarities with known or putative transporters and/or conserved domains of known transporter families (2, 5). It encompasses 410 amino acids with eight predicted (70) transmembrane domains (Fig. S1). The N- and C-terminal parts of *Pf*PMRT1 are both predicted (71) to be facing the cytosolic side of the parasite. Surface electrostatics indicate a clear polarity of *Pf*PMRT1 with negative charges facing the PV lumen and positive charges inside the parasite cytosol (Fig. S8F). The loops protruding into the PV lumen of *Pf*PMRT1 are generally larger than the cytosolic loops and possess stretches of negatively charged amino acids likely relevant for its transport function. Further functional characterization of *Pf*MRT1 will deliver insight into its transporter capabilities and physiological role.

Our phylogenetic analysis confirmed PMRT1 as unique for *Plasmodium* species, with high sequence conservation only within the *Laverania* subgenus (72). In line with data from genome-wide mutagenesis screens (63, 67) and reported failed knockout attempts in *P. yoelii* (69), we found that *Pf*PMRT1 is essential for parasite growth, as its functional inactivation resulted in growth arrest at the trophozoite stage accompanied by the accumulation of PPM-derived protrusions within the parasite. In contrast, conditional knockdown resulted only in a growth delay, indicating that minor residual *Pf*PMRT1 protein levels appear to be sufficient to promote parasite growth. This finding was validated by episomal expression of an allelic copy under the control of the weak *sf3a2* promoter (55) in the *Pf*PMRT1 knockout parasites. Additionally, we found that *Pf*PMRT1 is essential for early gametocytogenesis. Interestingly, the induction of the knockout at stages II to III had no effect on gametocytogenesis. This might be due to sufficient amounts of *Pf*PMRT1 already present at the PPM, but could also indicate that the function of the transporter is not required for later stage gametocyte maturation.

For future work, further functional and pharmacological characterization of this transporter will provide insights into its biological role in different stages of the parasite's life cycle, as transcriptomic data indicate—along with expression in blood stages (34, 35)—*Pf*PMRT1 is expressed in oocysts of *P. falciparum* (73, 74) and *P. berghei* (75).

MATERIALS AND METHODS

Cloning of plasmid constructs for parasite transfection. For endogenous tagging using the SLI system (41), homology regions (HRs) with lengths of 889 bp (*Pf*PMRT1; PF3D7_1135300), 905 bp (*Pf*FVRT1; PF3D7_0523800), 827 bp (*Pf*ZIP1; PF3D7_0609100), 873 bp (*Pf*DMT2; PF3D7_0716900), 877 bp (*Pf*MFS6; PF3D7_1440800), and 785 bp (*Pf*CDF; PF3D7_0715900) were amplified using 3D7 genomic DNA (gDNA) and cloned into pSLI-GFP-glmS (76) (derived from pSLI-GFP [41]), using the NotI/MluI restriction site. In order to generate *Pf*PMRT1-2×FKBP-GFP, a 1,000-bp-long HR was amplified using 3D7 gDNA and cloned into pSLI-2xFKBP-GFP (41).

For SLI-based targeted gene disruption (SLI-TGD) (41), HRs with lengths of 501 bp (*Pf*PMRT1), 378 bp (*Pf*FVRT1), 511 bp (*Pf*ZIP1), 399 bp (*Pf*DMT2), 396 bp (*Pf*MFS6), and 741 bp (*Pf*CDF) were amplified using 3D7 gDNA and cloned into the pSLI-TGD plasmid (41), using NotI and MluI restriction sites.

For conditional deletion of *Pf*PMRT1, the first 492 bp of the *Pf*PMRT1 gene were PCR amplified to append a first loxP site and a recodonized T2A skip peptide. The recodonized full-length coding region of *Pf*PMRT1 was synthesized (GenScript, Piscataway, NJ, USA) and PCR amplified with primers to add a second loxP site after the gene to obtain a second fragment. Both fragments were cloned into pSLI-3×HA (55), using NotI/SpeI and AvrII/XmaI sites. This resulted in plasmid pSLI-*Pf*PMRT1-loxP, and the resulting transgenic cell line after successful genomic modification was transfected with pSkip-Flox (41) using 2 μg/mL blasticidin S to obtain a line expressing the DiCre fragments (condΔPMRT1).

For complementation constructs, the recodonized *Pf*PMRT1 gene was PCR amplified using primers to append the TY1 sequence and cloned via XhoI and AvrII or KpnI into pEXP1comp (55) containing yDHODH as a resistance marker and different promoters (*nmd3* [PF3D7_0729300] and *sf3a2* [PF3D7_0619900]) driving expression of the expression cassette. This resulted in plasmids c-^{nmdr}*Pf*PMRT1-ty1 and c-^{sf3a2}*Pf*PMRT1-ty1.

*Pf*PMRT1 homologues of *P. vivax* (PVP01_0936100) (77) and *P. knowlesi* (PKNH_0933400) (78) were amplified from parasite gDNA and cloned into p^{nmd3}EXP1comp (55) via the XhoI/AvrII restriction site. For colocalization experiments, the plasmids pLyn-FRB-mCherry (41), P40PX-mCherry (44), pARL-^{crt}ACP-mCherry (46), pARL-^{ama1}ARO-mCherry (49), and pARL-^{ama1}AMA1-mCherry (51) were used. For conditional gametocyte induction, yDHODH was amplified by PCR from pARL-^{ama1}AMA1-mCherry-yDHODH (51) and cloned into GDV1-GFP-DD-hDHFR (59), using the XhoI/XhoI restriction site.

The oligonucleotides and plasmids used in this study are listed in Table S1 in the supplemental material.

***P. falciparum* culture and transfection.** Blood stages of *P. falciparum* 3D7 were cultured in human erythrocytes (O^+). Cultures were maintained at 37°C in an atmosphere of 1% O_2, 5% CO_2, and 94% N_2 using RPMI complete medium containing 0.5% Albumax according to standard protocols (79). To maintain synchronized parasites, cultures were treated with 5% sorbitol (80).

Induction of gametocytogenesis was done as previously described (58, 59). Briefly, GDV1-GFP-DD expression was achieved by addition of 4 μM shield-1 to the culture medium, and gametocyte cultures were treated with 50 mM *N*-acetyl-D-glucosamine (GlcNAc) for 5 days, starting 72 h post-shield-1 addition to eliminate asexual parasites (81). Alternatively, asexual ring stage cultures with >10% parasitemia were synchronized with sorbitol (80), cultured for 24 h, and treated with 50 mM *N*-acetyl-D-glucosamine (GlcNAc) (81) for 5 days.

For transfection, Percoll-purified (82) late schizont stage parasites were transfected with 50 μg of plasmid DNA, using Amaxa Nucleofector 2b (Lonza, Switzerland) as previously described (83). Transfectants were selected either using 4 nM WR99210 (Jacobus Pharmaceuticals), 2 μg/mL blasticidin S (Life Technologies, USA), or 0.9 μM DSM1 (84) (BEI Resources; https://www.beiresources.org). In order to select for parasites carrying the genomic modification using the SLI system (41), G418 (Sigma-Aldrich, St. Louis, MO) at a final concentration of 400 μg/mL was added to the 5% parasitemia culture. The selection process and testing for integration were performed as previously described (41).

For SLI-TGD, a total of six (*Pf*PMRT1, *Pf*DMT2, *Pf*ZIP1, and *Pf*CDF) or eight (*Pf*FVRT1 and *Pf*MFS6) independent 5-mL cultures containing the episomal plasmid were selected under G418 for at least 8 weeks.

Imaging and immunofluorescence analysis (IFA). Fluorescence images of infected erythrocytes were observed and captured using a Zeiss Axioskop 2 Plus microscope with a Hamamatsu digital camera (Model C4742-95), a Leica D6B fluorescence microscope equipped with a Leica DFC9000 GT camera and a Leica Plan Apochromat 100×/1.4 oil objective, or an Olympus FV3000 with a 100× MPLAPON oil objective (NA 1.4). Confocal microscopy was performed using a Leica SP8 microscope with laser excitation at 405 nm, 490 nm, and 550 nm for DAPI (4′,6-diamidino-2-phenylindole), GFP, and mCherry excitation, respectively. An HC PL APO 63× NA 1.4 oil immersion objective was used, and images were acquired with the HyVolution mode of the LASX microscopy software. After recording, images were deconvolved using Huygens (express deconvolution, setting "Standard").

Microscopy of unfixed *P. falciparum*-infected erythrocytes (IEs) was performed as previously described (85). Briefly, parasites were incubated in RPMI 1640 culture medium with Hoechst 33342 (Invitrogen) for 15 min at 37°C prior to imaging. Seven microliters of IEs was added on a glass slide, and the slide was covered with a coverslip. Control images of 3D7 wild-type parasites across the intraerythrocytic developmental cycle (IDC) are included in Fig. S8D and *E*.

BODIPY TR C5 ceramide (Invitrogen) staining was performed by adding the dye to 32-hpi parasites in a final concentration of 2.5 μM in RPMI as previously described (85). For DHE staining of the parasite cytosol (44), 80 μL of resuspended parasite culture was incubated with DHE at a final concentration of 4.5 μg/mL in the dark for 15 min prior to imaging.

IFAs were performed as described previously (86). Briefly, IEs were smeared on slides and air dried. Cells were fixed in 100% ice-cold methanol for 3 min at −20°C. Afterwards, cells were blocked with 5% milk powder for 30 min. Next, primary antibodies were diluted in phosphate-buffered saline (PBS)–3% milk powder and incubated for 2 h, followed by three washing steps in PBS. Secondary antibodies were applied for 2 h in PBS–3% milk powder containing 1 μg/mL Hoechst 33342 (Invitrogen) or DAPI (Roche) for nuclei staining, followed by 3 washes with PBS. One drop of mounting medium (Mowiol 4-88; Calbiochem) was added, and the slide was sealed with a coverslip for imaging.

To assess the localization of the endogenously HA-tagged *Pf*PMRT1, IFAs were performed in suspension with Compound 2-stalled schizonts (87) to distinguish protein located at the PPM from that located at the PVM, as previously described (55, 88). For this, trophozoite stages were treated with Compound 2 (1 μM) overnight, and arrested schizonts were harvested, washed in PBS, and fixed with 4% paraformaldehyde–0.0075% glutaraldehyde in PBS. Cells were permeabilized with 0.5% Triton X-100 in PBS, blocked with 3% bovine serum albumin (BSA) in PBS, and incubated overnight with primary antibodies diluted in 3% BSA in PBS. Cells were washed 3 times with PBS and incubated for 1 h with Alexa 488- or

Alexa 594-conjugated secondary antibodies specific for human and rat IgG (Invitrogen) diluted 1:2,000 in 3% BSA in PBS and containing 1 μg/mL DAPI. Cells were directly imaged after being washed 5 times with PBS.

The following antisera were used: 1:200 mouse anti-GFP clones 7.1 and 13.1 (Roche), 1:500 rat anti-HA clone 3F10 (Roche), 1:1,000 human anti-MSP1 (89), and 1:10,000 mouse anti-TY1 (Thermo Fischer Scientific, catalog no. MA5-23513). Contrast and intensities were linearly adjusted if necessary, and cropped images were assembled as panels using Fiji (90), Corel Photo-Paint X6, and Adobe Photoshop CC 2021.

Immunoblots. For immunoblotting, parasites were released from erythrocytes by incubation with 0.03% saponin in PBS for 10 min on ice, followed by three wash steps with Dulbecco's PBS (DPBS). Proteins were then extracted with lysis buffer (4% SDS, 0.5% Triton X-100, 0.5× DPBS in distilled water [dH_2O]) in the presence of protease cocktail inhibitor (Roche) and 1 mM phenylmethylsulfonyl fluoride (PMSF), followed by addition of reducing SDS sample buffer and 5 min of incubation at 55°C. Parasite proteins were separated on a 10% SDS-PAGE gel using standard procedures and transferred to a nitrocellulose membrane (Amersham Protran 0.45-μm pore NC; GE Healthcare) using a Trans-Blot device (Bio-Rad) according to manufacturer's instructions or to a nitrocellulose membrane (Licor) in a Tankblot device (Bio-Rad) using transfer buffer (0.192 M glycine, 0.1% SDS, 25 mM Tris-HCl [pH 8.0]) with 20% methanol.

Rabbit anti-aldolase (91) and anti-SBP1 (91) antibodies were diluted 1:2,000, mouse anti-GFP clone 7.1 and clone 13.1 (Roche) antibody was diluted 1:500 or 1:1,000, mouse anti-TY1 (Sigma) was diluted 1:20,000, rabbit anti-BIP (92) was diluted 1:2,500, and rat anti-HA clone 3F10 (Roche) antibody was diluted 1:1,000.

The chemiluminescent signal of the horseradish peroxidase (HRP)-coupled secondary antibodies (Dianova) was visualized using a Chemi Doc XRS imaging system (Bio-Rad) and processed with Image Lab Software 5.2 (Bio-Rad). To perform loading controls and ensure equal loading of parasite material, antialdolase antibodies were used. The corresponding immunoblots were incubated two times in stripping buffer (0.2 M glycine, 50 mM dithiothreitol [DTT], 0.05% Tween 20) at 55°C for 1 h and washed 3 times with Tris-buffered saline (TBS) for 10 min. For the Western blots shown in Fig. S8C, fluorescent signals of secondary goat anti-rabbit IgG coupled to IRDye 680CW and goat anti-mouse IgG coupled to IRDye 800CW were visualized using an Odyssey Fc imager by LI-COR Biosciences.

Growth assay. A flow cytometry-based assay adapted from previously published assays (44, 93) was performed. For this, parasite cultures were resuspended, and 20-μL samples were transferred to a centrifuge tube (Eppendorf AG, Germany). Eighty microliters of RPMI containing Hoechst 33342 and dihydroethidium (DHE) was added to obtain final concentrations of 5 μg/mL and 4.5 μg/mL, respectively. Samples were incubated for 20 min (protected from UV light) at room temperature, and parasitemia was determined using an LSRII flow cytometer by counting 100,000 events using the FACSDiva software (BD Biosciences) or using an ACEA NovoCyte flow cytometer.

Stage distribution assay. In order to obtain tightly synchronized parasite cultures, Percoll-purified schizonts (82) were cultured for 4 h together with fresh erythrocytes, followed by sorbitol synchronization and resulting in a 4-h age window of parasites. Next, the culture was divided into four dishes, and rapalog was added at a final concentration of 250 nM immediately to one dish and at 20 h postinvasion (hpi) and 32 hpi to the respective dishes. Giemsa smears and samples for flow cytometry were collected at the indicated time points. The parasitemia was determined using a flow cytometry assay, and the stages were determined microscopically by counting at least 50 infected erythrocytes per sample and time point.

Gametocyte stage distribution assay. Giemsa-stained blood smears 10 days postinduction of GDV1 expression were obtained, and at least 10 fields of view were recorded using a 63× objective per treatment and time point. Erythrocyte numbers were then determined using the automated Parasitemia software (http://www.gburri.org/parasitemia/), while the numbers of gametocytes and pycnotic and asexual parasites were determined manually in >1,800 erythrocytes per sample. This assay was done blind.

glmS-based knockdown. The glmS-based knockdown assay was adapted from previously published assays (42, 76). To induce knockdown, 2.5 or 5 mM glucosamine was added to highly synchronous early ring stage parasites. As a control, the same amount of glucosamine was also added to 3D7 wild-type parasites. For all analyses, the growth medium was changed daily, and fresh glucosamine was added every day.

Knockdown was quantified by fluorescence live cell microscopy at days 1 and 3 of the growth assay. Parasites of similar size were imaged, and fluorescence was captured with the same acquisition settings to obtain comparable measurements of the fluorescence intensity. Fluorescence intensity (integrated density) was measured with Fiji (90), and background was subtracted in each image. The data were analyzed with GraphPad Prism version 8.

glmS-based knockdown experiments in gametocytes were performed as described previously (94). Briefly, synchronized ring stage cultures were induced by the addition of shield-1. At day 3 postinduction, the culture was spilt into two dishes, and one dish was cultured in the presence of 2.5 mM glucosamine for the remaining 10 days. Knockdown was quantified by fluorescence live cell microscopy at days 7 and 10 postinduction, as described above, and gametocyte parasitemia was determined at day 10 postinduction by using the automated Parasitemia software (http://www.gburri.org/parasitemia/).

DiCre-mediated conditional knockout. The parasites containing the integrated pSLI-*Pf*PMRT1-loxP construct were transfected with pSkip-Flox (41) by using 2 μg/mL blasticidin S to obtain a line expressing the DiCre fragments. To induce excision, the tightly synchronized parasites (for a detailed description, see "Growth assay" above) were split into 2 dishes, and rapalog was added to one dish (Clontech, Mountain View, CA) to a final concentration of 250 nM. The untreated dish served as the control culture.

Excision was verified at the genomic level after 24 and 48 h of cultivation by PCR and at the protein level by Western blotting using anti-HA antibodies.

Phylogenetic analysis. A BLASTp search of the PMRT1 sequence (PlasmoDB [38]: PF3D7_1135300; UniProt accession no. Q8II12) was performed against the nr database (9 May 2021) using Geneious Prime 2021.2.2 (https://www.geneious.com) and an *E* value of 10e−0 (BLOSUM62 substitution matrix). BLAST hits were filtered for sequences from taxa represented in the currently favored haemosporidian parasite phylogeny (95). The phylogeny derived from an amino acid alignment using Bayesian framework with a partitioned supermatrix and a relaxed molecular clock (18_amino_acid_partitioned_BEAST_relaxed_clock_no_outgroup.tre) (95) was visualized with associated data using the R package ggtree v3.3.0.900 (96, 97). A multiple-protein-sequence alignment of PMRT1 and homologous sequences was performed using MAFFT v7.490 (98) with the G-INS-I algorithm to obtain a highly accurate alignment. Protein statistics were calculated using Geneious Prime 2021.2.2 (https://www.geneious.com) and EMBOSS pepstats v6.6.0.0 (99).

Prediction of protein structures. AlphaFold structure predictions (39) were retrieved from https://alphafold.ebi.ac.uk and the PDB and used for a DALI protein structure homology search (40). PyMOL Molecular Graphics System v2.5.2 Schrödinger was used for visualization of all structures, generation of figures, and the calculation of the root mean square deviation (RMSD) between the predicted crystal structure of *Pf*PMRT1 and the Maquette-3 protein (PDB accession no. 5vjt) (60) by cealign. The Adaptive Poisson-Boltzmann Solver (APBS) within PyMOL was used to predict the surface electrostatics of *Pf*PMRT1.

Parasite icons were generated using BioRender (biorender.com), plasmids and oligonucleotides were designed using ApE (100), and statistical analysis was performed using GraphPad Prism version 8 (GraphPad Software, USA).

SUPPLEMENTAL MATERIAL

Supplemental material is available online only.

FIG S1, TIF file, 0.9 MB.

FIG S2, TIF file, 2.8 MB.

FIG S3, TIF file, 1.4 MB.

FIG S4, TIF file, 2.7 MB.

FIG S5, TIF file, 0.4 MB.

FIG S6, TIF file, 1.6 MB.

FIG S7, TIF file, 1.7 MB.

FIG S8, TIF file, 1.3 MB.

TABLE S1, PDF file, 0.1 MB.

ACKNOWLEDGMENTS

We thank Michael Filarsky for providing the pHcamGDV1-GFP-DD_hDHFR plasmid, Egbert Tannich for providing *P. vivax* and *P. knowlesi* gDNA, Mike Blackman for the anti-MSP1 antibody, Jacobus Pharmaceuticals for WR99210, Greg Burri for the parasitemia software, and the Advanced Light and Fluorescence Microscopy (ALFM) facility at the Centre for Structural Systems Biology (CSSB), in particular Roland Thuenauer, for support with light microscopy image recording and analysis. DSM1 (MRA-1161) was obtained from MR4/BEI Resources, NIAID, NIH. Furthermore, we thank Maria Rosenthal for help with the visualization of the predicted protein structures.

A. Bachmann and J. S. Wichers were funded by the German Research Foundation (DFG) grant BA 5213/3-1. Partnership of Universität Hamburg and DESY (PIER) project ID PIF-2018-87 (J. Strauss, C. Löw, and T.-W. Gilberger), CSSB Seed grant KIF 2019/002 (T.-W. Gilberger), a Hospital Research Foundation Fellowship (D. Wilson), and the DAAD/Universities Australia Joint Research Co-operation Scheme (T.-W. Gilberger, D. Wilson, and B. Liffner). I. Henshall and B. Liffner were supported by Australian Government Research Training Stipend. J. Yu-Strzelczyk., S. Gao, and G. Nagel were funded by DFG Projektnummer 374031971 TRR 240 A04 and 417451587. J. Stäcker thanks the Jürgen Manchot Stiftung for funding, and P. Mesén-Ramirez and T. Spielmann acknowledge funding by the DFG (SP1209/4-1).

Conceptualization, J. S. Wichers, T.-W. Gilberger, A. Bachmann, and J. Strauss; Methodology, G. Nagel and S. Gao; Investigation, J. S. Wichers, P. Mesén-Ramirez, J. Yu-Strzelczyk, G. Fuchs; J. Stäcker, H. von Thien., A. Alder, I. Henshall, and B. Liffner; Formal Analysis, J. Strauss; Writing – Original Manuscript: J. S. Wichers, A. Bachmann, J. Strauss, and D. Wilson; Writing – Review & Editing: J. S. Wichers, P. Mesén-Ramirez, T.-W. Gilberger, A. Bachmann, J. Strauss, and D. Wilson; Funding Acquisition, D. Wilson, C. Löw,

T.-W. Gilberger, A. Bachmann, and J. Strauss; Resources, T.-W. Gilberger; Project Administration, T.-W. Gilberger, A. Bachmann, and J. Strauss; Supervision, D. Wilson, T. Spielmann, S. Gao, T.-W. Gilberger, and A. Bachmann.

All authors read and approved the manuscript.

REFERENCES

1. Martin RE, Henry RI, Abbey JL, Clements JD, Kirk K. 2005. The "permeome" of the malaria parasite: an overview of the membrane transport proteins of Plasmodium falciparum. Genome Biol 6:R26. https://doi.org/10.1186/gb-2005-6-3-r26.
2. Martin RE. 2020. The transportome of the malaria parasite. Biol Rev Camb Philos Soc 95:305–332. https://doi.org/10.1111/brv.12565.
3. Gardner MJ, Hall N, Fung E, White O, Berriman M, Hyman RW, Carlton JM, Pain A, Nelson KE, Bowman S, Paulsen IT, James K, Eisen JA, Rutherford K, Salzberg SL, Craig A, Kyes S, Chan M-S, Nene V, Shallom SJ, Suh B, Peterson J, Angiuoli S, Pertea M, Allen J, Selengut J, Haft D, Mather MW, Vaidya AB, Martin DMA, Fairlamb AH, Fraunholz MJ, Roos DS, Ralph SA, McFadden GI, Cummings LM, Subramanian GM, Mungall C, Venter JC, Carucci DJ, Hoffman SL, Newbold C, Davis RW, Fraser CM, Barrell B. 2002. Genome sequence of the human malaria parasite Plasmodium falciparum. Nature 419:498–511. https://doi.org/10.1038/nature01097.
4. Martin RE, Ginsburg H, Kirk K. 2009. Membrane transport proteins of the malaria parasite. Mol Microbiol 74:519–528. https://doi.org/10.1111/j.1365-2958.2009.06863.x.
5. Weiner J, Kooij TWA. 2016. Phylogenetic profiles of all membrane transport proteins of the malaria parasite highlight new drug targets. Microb Cell 3:511–521. https://doi.org/10.15698/mic2016.10.534.
6. Garten M, Nasamu AS, Niles JC, Zimmerberg J, Goldberg DE, Beck JR. 2018. EXP2 is a nutrient-permeable channel in the vacuolar membrane of Plasmodium and is essential for protein export via PTEX. Nat Microbiol 3:1090–1098. https://doi.org/10.1038/s41564-018-0222-7.
7. Desai SA, Krogstad DJ, McCleskey EW. 1993. A nutrient-permeable channel on the intraerythrocytic malaria parasite. Nature 362:643–646. https://doi.org/10.1038/362643a0.
8. Nguitragool W, Bokhari AAB, Pillai AD, Rayavara K, Sharma P, Turpin B, Aravind L, Desai SA. 2011. Malaria parasite clag3 genes determine channel-mediated nutrient uptake by infected red blood cells. Cell 145:665–677. https://doi.org/10.1016/j.cell.2011.05.002.
9. Dean P, Major P, Nakjang S, Hirt RP, Martin Embley T. 2014. Transport proteins of parasitic protists and their role in nutrient salvage. Front Plant Sci 5:153. https://doi.org/10.3389/fpls.2014.00153.
10. Foote SJ, Thompson JK, Cowman AF, Kemp DJ. 1989. Amplification of the multidrug resistance gene in some chloroquine-resistant isolates of P. falciparum. Cell 57:921–930. https://doi.org/10.1016/0092-8674(89)90330-9.
11. Fidock DA, Nomura T, Talley AK, Cooper RA, Dzekunov SM, Ferdig MT, Ursos LMB, Bir Singh Sidhu A, Naudé B, Deitsch KW, Su XZ, Wootton JC, Roepe PD, Wellems TE. 2000. Mutations in the P. falciparum digestive vacuole transmembrane protein PfCRT and evidence for their role in chloroquine resistance. Mol Cell 6:861–871. https://doi.org/10.1016/S1097-2765(05)00077-8.
12. Veiga MI, Dhingra SK, Henrich PP, Straimer J, Gnädig N, Uhlemann AC, Martin RE, Lehane AM, Fidock DA. 2016. Globally prevalent PfMDR1 mutations modulate Plasmodium falciparum susceptibility to artemisinin-based combination therapies. Nat Commun 7:11553. https://doi.org/10.1038/ncomms11553.
13. Rijpma SR, Van Der Velden M, Bilos A, Jansen RS, Mahakena S, Russel FGM, Sauerwein RW, Van De Wetering K, Koenderink JB. 2016. MRP1 mediates folate transport and antifolate sensitivity in Plasmodium falciparum. FEBS Lett 590:482–492. https://doi.org/10.1002/1873-3468.12079.
14. Mesén-Ramírez P, Bergmann B, Elhabiri M, Zhu L, von Thien H, Castro-Peña C, Gilberger T-W, Davioud-Charvet E, Bozdech Z, Bachmann A, Spielmann T. 2021. The parasitophorous vacuole nutrient pore is critical for drug access in malaria parasites and modulates the fitness cost of artemisinin resistance. Cell Host Microbe 29:1774–1787.e9. https://doi.org/10.1016/j.chom.2021.11.002.
15. Cowman AF, Galatis D, Thompson JK. 1994. Selection for mefloquine resistance in Plasmodium falciparum is linked to amplification of the pfmdr1 gene and cross-resistance to halofantrine and quinine. Proc Natl Acad Sci U S A 91:1143–1147. https://doi.org/10.1073/pnas.91.3.1143.
16. Mok S, Liong KY, Lim EH, Huang X, Zhu L, Preiser PR, Bozdech Z. 2014. Structural polymorphism in the promoter of pfmrp2 confers Plasmodium falciparum tolerance to quinoline drugs. Mol Microbiol 91:918–934. https://doi.org/10.1111/mmi.12505.
17. Lim MYX, LaMonte G, Lee MCS, Reimer C, Tan BH, Corey V, Tjahjadi BF, Chua A, Nachon M, Wintjens R, Gedeck P, Malleret B, Renia L, Bonamy GMC, Ho PCL, Yeung BKS, Chow ED, Lim L, Fidock DA, Diagana TT, Winzeler EA, Bifani P. 2016. UDP-galactose and acetyl-CoA transporters as Plasmodium multidrug resistance genes. Nat Microbiol 1:16166. https://doi.org/10.1038/nmicrobiol.2016.166.
18. Richards SN, Nash MN, Baker ES, Webster MW, Lehane AM, Shafik SH, Martin RE. 2016. Molecular mechanisms for drug hypersensitivity induced by the malaria parasite's chloroquine resistance transporter. PLoS Pathog 12:e1005725. https://doi.org/10.1371/journal.ppat.1005725.
19. Cowell AN, Istvan ES, Lukens AK, Gomez-Lorenzo MG, Vanaerschot M, Sakata-Kato T, Flannery EL, Magistrado P, Owen E, Abraham M, La Monte G, Painter HJ, Williams RM, Franco V, Linares M, Arriaga I, Bopp S, Corey VC, Gnädig NF, Coburn-Flynn O, Reimer C, Gupta P, Murithi JM, Moura PA, Fuchs O, Sasaki E, Kim SW, Teng CH, Wang LT, Akidil A, Adjalley S, Willis PA, Siegel D, Tanaseichuk O, Zhong Y, Zhou Y, Llinás M, Ottilie S, Gamo FJ, Lee MCS, Goldberg DE, Fidock DA, Wirth DF, Winzeler EA. 2018. Mapping the malaria parasite druggable genome by using in vitro evolution and chemogenomics. Science 359:191–199. https://doi.org/10.1126/science.aan4472.
20. Rocamora F, Gupta P, Istvan ES, Luth MR, Carpenter EF, Kümpornsin K, Sasaki E, Calla J, Mittal N, Carolino K, Owen E, Llinás M, Ottilie S, Goldberg DE, Lee MCS, Winzeler EA. 2021. PfMFR3: a multidrug-resistant modulator in Plasmodium falciparum. ACS Infect Dis 7:811–825. https://doi.org/10.1021/acsinfecdis.0c00676.
21. Kirk K. 2004. Channels and transporters as drug targets in the Plasmodium-infected erythrocyte. Acta Trop 89:285–298. https://doi.org/10.1016/j.actatropica.2003.10.002.
22. Koenderink JB, Kavishe RA, Rijpma SR, Russel FGM. 2010. The ABCs of multidrug resistance in malaria. Trends Parasitol 26:440–446. https://doi.org/10.1016/j.pt.2010.05.002.
23. Murithi JM, Deni I, Pasaje CFA, Okombo J, Bridgford JL, Gnädig NF, Edwards RL, Yeo T, Mok S, Burkhard AY, Coburn-Flynn O, Istvan ES, Sakata-Kato T, Gomez-Lorenzo MG, Cowell AN, Wicht KJ, Le Manach C, Kalantarov GF, Dey S, Duffey M, Laleu B, Lukens AK, Ottilie S, Vanaerschot M, Trakht IN, Gamo F-J, Wirth DF, Goldberg DE, Odom John AR, Chibale K, Winzeler EA, Niles JC, Fidock DA. 2021. The Plasmodium falciparum ABC transporter ABCI3 confers parasite strain-dependent pleiotropic antimalarial drug resistance. Cell Chem Biol https://doi.org/10.1016/j.chembiol.2021.06.006.
24. Counihan NA, Modak JK, de Koning-Ward TF. 2021. How malaria parasites acquire nutrients from their host. Front Cell Dev Biol 9:649184. https://doi.org/10.3389/fcell.2021.649184.
25. Saliba KJ, Horner HA, Kirk K. 1998. Transport and metabolism of the essential vitamin pantothenic acid in human erythrocytes infected with the malaria parasite Plasmodium falciparum. J Biol Chem 273:10190–10195. https://doi.org/10.1074/jbc.273.17.10190.
26. Gulati S, Ekland EH, Ruggles KV, Chan RB, Jayabalasingham B, Zhou B, Mantel PY, Lee MCS, Spottiswoode N, Coburn-Flynn O, Hjelmqvist D, Worgall TS, Marti M, Di Paolo G, Fidock DA. 2015. Profiling the essential nature of lipid metabolism in asexual blood and gametocyte stages of Plasmodium falciparum. Cell Host Microbe 18:371–381. https://doi.org/10.1016/j.chom.2015.08.003.
27. Ben Mamoun C, Prigge ST, Vial H. 2010. Targeting the lipid metabolic pathways for the treatment of malaria. Drug Dev Res 71:44–55. https://doi.org/10.1002/ddr.20347.
28. Garten M, Beck JR. 2021. Structured to conquer: transport across the Plasmodium parasitophorous vacuole. Curr Opin Microbiol 63:181–188. https://doi.org/10.1016/j.mib.2021.07.010.

29. Kloehn J, Lacour CE, Soldati-Favre D. 2021. The metabolic pathways and transporters of the plastid organelle in Apicomplexa. Curr Opin Microbiol 63:250–258. https://doi.org/10.1016/j.mib.2021.07.016.
30. Beck JR, Ho CM. 2021. Transport mechanisms at the malaria parasite-host cell interface. PLoS Pathog 17:e1009394. https://doi.org/10.1371/journal.ppat.1009394.
31. Kenthirapalan S, Waters AP, Matuschewski K, Kooij TWA. 2016. Functional profiles of orphan membrane transporters in the life cycle of the malaria parasite. Nat Commun 7:10519. https://doi.org/10.1038/ncomms10519.
32. Sayers CP, Mollard V, Buchanan HD, McFadden GI, Goodman CD. 2018. A genetic screen in rodent malaria parasites identifies five new apicoplast putative membrane transporters, one of which is essential in human malaria parasites. Cell Microbiol 20:e12789. https://doi.org/10.1111/cmi.12789.
33. Ginsburg H. 2006. Progress in in silico functional genomics: the malaria Metabolic Pathways database. Trends Parasitol 22:238–240. https://doi.org/10.1016/j.pt.2006.04.008.
34. Otto TD, Wilinski D, Assefa S, Keane TM, Sarry LR, Böhme U, Lemieux J, Barrell B, Pain A, Berriman M, Newbold C, Llinás M. 2010. New insights into the blood-stage transcriptome of Plasmodium falciparum using RNA-Seq. Mol Microbiol 76:12–24. https://doi.org/10.1111/j.1365-2958.2009.07026.x.
35. Wichers JS, Scholz JAM, Strauss J, Witt S, Lill A, Ehnold LI, Neupert N, Liffner B, Lühken R, Petter M, Lorenzen S, Wilson DW, Löw C, Lavazec C, Bruchhaus I, Tannich E, Gilberger TW, Bachmann A. 2019. Dissecting the gene expression, localization, membrane topology, and function of the Plasmodium falciparum STEVOR protein family. mBio 10:e01500-19. https://doi.org/10.1128/mBio.01500-19.
36. Treeck M, Sanders JL, Elias JE, Boothroyd JC. 2011. The phosphoproteomes of Plasmodium falciparum and toxoplasma gondii reveal unusual adaptations within and beyond the parasites' boundaries. Cell Host Microbe 10:410–419. https://doi.org/10.1016/j.chom.2011.09.004.
37. Pease BN, Huttlin EL, Jedrychowski MP, Talevich E, Harmon J, Dillman T, Kannan N, Doerig C, Chakrabarti R, Gygi SP, Chakrabarti D. 2013. Global analysis of protein expression and phosphorylation of three stages of Plasmodium falciparum intraerythrocytic development. J Proteome Res 12:4028–4045. https://doi.org/10.1021/pr400394g.
38. Aurrecoechea C, Brestelli J, Brunk BP, Dommer J, Fischer S, Gajria B, Gao X, Gingle A, Grant G, Harb OS, Heiges M, Innamorato F, Iodice J, Kissinger JC, Kraemer E, Li W, Miller JA, Nayak V, Pennington C, Pinney DF, Roos DS, Ross C, Stoeckert CJ, Treatman C, Wang H. 2009. PlasmoDB: a functional genomic database for malaria parasites. Nucleic Acids Res 37:D539–D543. https://doi.org/10.1093/nar/gkn814.
39. Jumper J, Evans R, Pritzel A, Green T, Figurnov M, Ronneberger O, Tunyasuvunakool K, Bates R, Žídek A, Potapenko A, Bridgland A, Meyer C, Kohl SAA, Ballard AJ, Cowie A, Romera-Paredes B, Nikolov S, Jain R, Adler J, Back T, Petersen S, Reiman D, Clancy E, Zielinski M, Steinegger M, Pacholska M, Berghammer T, Bodenstein S, Silver D, Vinyals O, Senior AW, Kavukcuoglu K, Kohli P, Hassabis D. 2021. Highly accurate protein structure prediction with AlphaFold. Nature 596:583–589. https://doi.org/10.1038/s41586-021-03819-2.
40. Holm L. 2020. DALI and the persistence of protein shape. Protein Sci 29:128–140. https://doi.org/10.1002/pro.3749.
41. Birnbaum J, Flemming S, Reichard N, Soares AB, Mesén-Ramírez P, Jonscher E, Bergmann B, Spielmann T. 2017. A genetic system to study Plasmodium falciparum protein function. Nat Methods 14:450–456. https://doi.org/10.1038/nmeth.4223.
42. Prommana P, Uthaipibull C, Wongsombat C, Kamchonwongpaisan S, Yuthavong Y, Knuepfer E, Holder AA, Shaw PJ. 2013. Inducible knockdown of Plasmodium gene expression using the glmS ribozyme. PLoS One 8:e73783. https://doi.org/10.1371/journal.pone.0073783.
43. Tawk L, Chicanne G, Dubremetz J-F, Richard V, Payrastre B, Vial HJ, Roy C, Wengelnik K. 2010. Phosphatidylinositol 3-phosphate, an essential lipid in Plasmodium, localizes to the food vacuole membrane and the apicoplast. Eukaryot Cell 9:1519–1530. https://doi.org/10.1128/EC.00124-10.
44. Jonscher E, Flemming S, Schmitt M, Sabitzki R, Reichard N, Birnbaum J, Bergmann B, Höhn K, Spielmann T. 2019. PfVPS45 is required for host cell cytosol uptake by malaria blood stage parasites. Cell Host Microbe 25:166–173.e5. https://doi.org/10.1016/j.chom.2018.11.010.
45. Waller RF, Reed MB, Cowman AF, McFadden GI. 2000. Protein trafficking to the plastid of Plasmodium falciparum is via the secretory pathway. EMBO J 19:1794–1802. https://doi.org/10.1093/emboj/19.8.1794.
46. Birnbaum J, Scharf S, Schmidt S, Jonscher E, Hoeijmakers WAM, Flemming S, Toenhake CG, Schmitt M, Sabitzki R, Bergmann B, Fröhlke U, Mesén-Ramírez P, Blancke Soares A, Herrmann H, Bártfai R, Spielmann T. 2020. A Kelch13-defined endocytosis pathway mediates artemisinin resistance in malaria parasites. Science 367:51–59. https://doi.org/10.1126/science.aax4735.
47. Inoue T, Do Heo W, Grimley JS, Wandless TJ, Meyer T. 2005. An inducible translocation strategy to rapidly activate and inhibit small GTPase signaling pathways. Nat Methods 2:415–418. https://doi.org/10.1038/nmeth763.
48. Geiger M, Brown C, Wichers JS, Strauss J, Lill A, Thuenauer R, Liffner B, Wilcke L, Lemcke S, Heincke D, Pazicky S, Bachmann A, Löw C, Wilson DW, Filarsky M, Burda P-C, Zhang K, Junop M, Gilberger TW. 2020. Structural insights into PfARO and characterization of its interaction with PfAIP. J Mol Biol 432:878–896. https://doi.org/10.1016/j.jmb.2019.12.024.
49. Cabrera A, Herrmann S, Warszta D, Santos JM, John Peter AT, Kono M, Debrouver S, Jacobs T, Spielmann T, Ungermann C, Soldati-Favre D, Gilberger TW. 2012. Dissection of minimal sequence requirements for rhoptry membrane targeting in the malaria parasite. Traffic 13:1335–1350. https://doi.org/10.1111/j.1600-0854.2012.01394.x.
50. Peterson MG, Marshall VM, Smythe JA, Crewther PE, Lew A, Silva A, Anders RF, Kemp DJ. 1989. Integral membrane protein located in the apical complex of Plasmodium falciparum. Mol Cell Biol 9:3151–3154. https://doi.org/10.1128/mcb.9.7.3151-3154.1989.
51. Wichers JS, Wunderlich J, Heincke D, Pazicky S, Strauss J, Schmitt M, Kimmel J, Wilcke L, Scharf S, von Thien H, Burda P, Spielmann T, Löw C, Filarsky M, Bachmann A, Gilberger TW. 2021. Identification of novel inner membrane complex and apical annuli proteins of the malaria parasite Plasmodium falciparum. Cell Microbiol 23:e13341. https://doi.org/10.1111/cmi.13341.
52. Jullien N, Goddard I, Selmi-Ruby S, Fina J-L, Cremer H, Herman J-P. 2007. Conditional transgenesis using dimerizable Cre (DiCre). PLoS One 2:e1355. https://doi.org/10.1371/journal.pone.0001355.
53. Andenmatten N, Egarter S, Jackson AJ, Jullien N, Herman JP, Meissner M. 2013. Conditional genome engineering in Toxoplasma gondii uncovers alternative invasion mechanisms. Nat Methods 10:125–127. https://doi.org/10.1038/nmeth.2301.
54. Holder AA, Lockyer MJ, Odink KG, Sandhu JS, Riveros-Moreno V, Nicholls SC, Hillman Y, Davey LS, Tizard MLV, Schwarz RT, Freeman RR. 1985. Primary structure of the precursor to the three major surface antigens of Plasmodium falciparum merozoites. Nature 317:270–273. https://doi.org/10.1038/317270a0.
55. Mesén-Ramírez P, Bergmann B, Tran TT, Garten M, Stäcker J, Naranjo-Prado I, Höhn K, Zimmerberg J, Spielmann T. 2019. EXP1 is critical for nutrient uptake across the parasitophorous vacuole membrane of malaria parasites. PLoS Biol 17:e3000473. https://doi.org/10.1371/journal.pbio.3000473.
56. López-Barragán MJ, Lemieux J, Quiñones M, Williamson KC, Molina-Cruz A, Cui K, Barillas-Mury C, Zhao K, Zhuan Su X. 2011. Directional gene expression and antisense transcripts in sexual and asexual stages of Plasmodium falciparum. BMC Genomics 12:587. https://doi.org/10.1186/1471-2164-12-587.
57. Lasonder E, Rijpma SR, Van Schaijk BCL, Hoeijmakers WAM, Kensche PR, Gresnigt MS, Italiaander A, Vos MW, Woestenenk R, Bousema T, Mair GR, Khan SM, Janse CJ, Bártfai R, Sauerwein RW. 2016. Integrated transcriptomic and proteomic analyses of P. falciparum gametocytes: molecular insight into sex-specific processes and translational repression. Nucleic Acids Res 44:6087–6101. https://doi.org/10.1093/nar/gkw536.
58. Boltryk SD, Passecker A, Alder A, Carrington E, van de Vegte-Bolmer M, van Gemert G-J, van der Starre A, Beck H-P, Sauerwein RW, Kooij TWA, Brancucci NMB, Proellochs NI, Gilberger T-W, Voss TS. 2021. CRISPR/Cas9-engineered inducible gametocyte producer lines as a valuable tool for Plasmodium falciparum malaria transmission research. Nat Commun 12:4806. https://doi.org/10.1038/s41467-021-24954-4.
59. Filarsky M, Fraschka SA, Niederwieser I, Brancucci NMB, Carrington E, Carrió E, Moes S, Jenoe P, Bártfai R, Voss TS. 2018. GDV1 induces sexual commitment of malaria parasites by antagonizing HP1-dependent gene silencing. Science 359:1259–1263. https://doi.org/10.1126/science.aan6042.
60. Ennist NM, Stayrook SE, Dutton PL, Moser CC. 2017. 5VJT: de novo photosynthetic reaction center protein equipped with heme B and Zn(II) cations. https://doi.org/10.2210/pdb5VJT/pdb.
61. Wunderlich J, Rohrbach P, Dalton JP. 2012. The malaria digestive vacuole. Front Biosci 4:1424–1448. https://doi.org/10.2741/s344.
62. Tabuchi M, Yoshimori T, Yamaguchi K, Yoshida T, Kishi F. 2000. Human NRAMP2/DMT1, which mediates iron transport across endosomal membranes, is localized to late endosomes and lysosomes in HEp-2 cells. J Biol Chem 275:22220–22228. https://doi.org/10.1074/jbc.M001478200.

63. Zhang M, Wang C, Otto TD, Oberstaller J, Liao X, Adapa SR, Udenze K, Bronner IF, Casandra D, Mayho M, Brown J, Li S, Swanson J, Rayner JC, Jiang RHY, Adams JH. 2018. Uncovering the essential genes of the human malaria parasite Plasmodium falciparum by saturation mutagenesis. Science 360:eaap7847. https://doi.org/10.1126/science.aap7847.
64. Kennedy K, Cobbold SA, Hanssen E, Birnbaum J, Spillman NJ, McHugh E, Brown H, Tilley L, Spielmann T, McConville MJ, Ralph SA. 2019. Delayed death in the malaria parasite Plasmodium falciparum is caused by disruption of prenylation-dependent intracellular trafficking. PLoS Biol 17: e3000376. https://doi.org/10.1371/journal.pbio.3000376.
65. Pasaje CFA, Cheung V, Kennedy K, Lim EE, Baell JB, Griffin MDW, Ralph SA. 2016. Selective inhibition of apicoplast tryptophanyl-tRNA synthetase causes delayed death in Plasmodium falciparum. Sci Rep 6:27531–27513. https://doi.org/10.1038/srep27531.
66. Yeh E, DeRisi JL. 2011. Chemical rescue of malaria parasites lacking an apicoplast defines organelle function in blood-stage plasmodium falciparum. PLoS Biol 9:e1001138. https://doi.org/10.1371/journal.pbio.1001138.
67. Bushell E, Gomes AR, Sanderson T, Anar B, Girling G, Herd C, Metcalf T, Modrzynska K, Schwach F, Martin RE, Mather MW, McFadden GI, Parts L, Rutledge GG, Vaidya AB, Wengelnik K, Rayner JC, Billker O. 2017. Functional profiling of a Plasmodium genome reveals an abundance of essential genes. Cell 170:260–272.e8. https://doi.org/10.1016/j.cell.2017.06.030.
68. Chasen NM, Stasic AJ, Asady B, Coppens I, Moreno SNJ. 2019. The vacuolar zinc transporter TgZnT protects Toxoplasma gondii from zinc toxicity. mSphere 4:e00086-19. https://doi.org/10.1128/mSphere.00086-19.
69. Jiang Y, Wei J, Cui H, Liu C, Zhi Y, Jiang Z, Li Z, Li S, Yang Z, Wang X, Qian P, Zhang C, Zhong C, Su X, Yuan J. 2020. An intracellular membrane protein GEP1 regulates xanthurenic acid induced gametogenesis of malaria parasites. Nat Commun 11:1764. https://doi.org/10.1038/s41467-020-15479-3.
70. Sonnhammer EL, von Heijne G, Krogh A. 1998. A hidden Markov model for predicting transmembrane helices in protein sequences. Proc Int Conf Intell Syst Mol Biol 6:175–182.
71. Käll L, Krogh A, Sonnhammer ELL. 2004. A combined transmembrane topology and signal peptide prediction method. J Mol Biol 338:1027–1036. https://doi.org/10.1016/j.jmb.2004.03.016.
72. Liu W, Sundararaman SA, Loy DE, Learn GH, Li Y, Plenderleith LJ, Ndjango JBN, Speede S, Atencia R, Cox D, Shaw GM, Ayouba A, Peeters M, Rayner JC, Hahn BH, Sharp PM. 2016. Multigenomic delineation of Plasmodium species of the Laverania subgenus infecting wild-living chimpanzees and gorillas. Genome Biol Evol 8:1929–1939. https://doi.org/10.1093/gbe/evw128.
73. Zanghì G, Vembar SS, Baumgarten S, Ding S, Guizetti J, Bryant JM, Mattei D, Jensen ATR, Rénia L, Goh YS, Sauerwein R, Hermsen CC, Franetich J-F, Bordessoulles M, Silvie O, Soulard V, Scatton O, Chen P, Mecheri S, Mazier D, Scherf A. 2018. A specific PfEMP1 is expressed in P falciparum sporozoites and plays a role in hepatocyte infection. Cell Rep 22: 2951–2963. https://doi.org/10.1016/j.celrep.2018.02.075.
74. Gómez-Díaz E, Yerbanga RS, Lefèvre T, Cohuet A, Rowley MJ, Ouedraogo JB, Corces VG. 2017. Epigenetic regulation of Plasmodium falciparum clonally variant gene expression during development in Anopheles gambiae. Sci Rep 7:40655. https://doi.org/10.1038/srep40655.
75. Howick VM, Russell AJC, Andrews T, Heaton H, Reid AJ, Natarajan K, Butungi H, Metcalf T, Verzier LH, Rayner JC, Berriman M, Herren JK, Billker O, Hemberg M, Talman AM, Lawniczak MKN. 2019. The Malaria Cell Atlas: single parasite transcriptomes across the complete Plasmodium life cycle. Science 365:eaaw2619. https://doi.org/10.1126/science.aaw2619.
76. Burda P-C, Crosskey T, Lauk K, Zurborg A, Söhnchen C, Liffner B, Wilcke L, Strauss J, Jeffries CM, Svergun DI, Wilson DW, Wilmanns M, Gilberger T-W, Pietsch E, Strauss J, Jeffries CM, Svergun DI, Wilson DW, Wilmanns M, Gilberger T-W. 2020. Structure-based identification and functional characterization of a lipocalin in the malaria parasite Plasmodium falciparum. Cell Rep 31:107817. https://doi.org/10.1016/j.celrep.2020.107817.
77. Auburn S, Böhme U, Steinbiss S, Trimarsanto H, Hostetler J, Sanders M, Gao Q, Nosten F, Newbold CI, Berriman M, Price RN, Otto TD. 2016. A new Plasmodium vivax reference sequence with improved assembly of the subtelomeres reveals an abundance of pir genes. Wellcome Open Res 1:4. https://doi.org/10.12688/wellcomeopenres.9876.1.
78. Pain A, Böhme U, Berry AE, Mungall K, Finn RD, Jackson AP, Mourier T, Mistry J, Pasini EM, Aslett MA, Balasubrammaniam S, Borgwardt K, Brooks K, Carret C, Carver TJ, Cherevach I, Chillingworth T, Clark TG, Galinski MR, Hall N, Harper D, Harris D, Hauser H, Ivens A, Janssen CS, Keane T, Larke N, Lapp S, Marti M, Moule S, Meyer IM, Ormond D, Peters N, Sanders M, Sanders S, Sargeant TJ, Simmonds M, Smith F, Squares R, Thurston S, Tivey AR, Walker D, White B, Zuiderwijk E, Churcher C, Quail MA, Cowman AF, Turner CMR, Rajandream MA, Kocken CHM, Thomas AW, Newbold CI, et al. 2008. The genome of the simian and human malaria parasite Plasmodium knowlesi. Nature 455:799–803. https://doi.org/10.1038/nature07306.
79. Trager W, Jensen JB. 1997. Continuous culture of Plasmodium falciparum: its impact on malaria research. Int J Parasitol 27:989–1006. https://doi.org/10.1016/s0020-7519(97)00080-5.
80. Lambros C, Vanderberg JP. 1979. Synchronization of Plasmodium falciparum erythrocytic stages in culture. J Parasitol 65:418–420. https://doi.org/10.2307/3280287.
81. Ponnudurai T, Lensen AHW, Meis JFGM, Meuwissen JHE. 1986. Synchronization of Plasmodium falciparum gametocytes using an automated suspension culture system. Parasitology 93:263–274. https://doi.org/10.1017/S003118200005143X.
82. Rivadeneira E, Wasserman M, Espinal C. 1983. Separation and concentration of schizonts of Plasmodium falciparum by Percoll gradients. J Protozool 30:367–370. https://doi.org/10.1111/j.1550-7408.1983.tb02932.x.
83. Moon RW, Hall J, Rangkuti F, Ho YS, Almond N, Mitchell GH, Pain A, Holder AA, Blackman MJ. 2013. Adaptation of the genetically tractable malaria pathogen Plasmodium knowlesi to continuous culture in human erythrocytes. Proc Natl Acad Sci U S A 110:531–536. https://doi.org/10.1073/pnas.1216457110.
84. Ganesan SM, Morrisey JM, Ke H, Painter HJ, Laroiya K, Phillips MA, Rathod PK, Mather MW, Vaidya AB. 2011. Yeast dihydroorotate dehydrogenase as a new selectable marker for Plasmodium falciparum transfection. Mol Biochem Parasitol 177:29–34. https://doi.org/10.1016/j.molbiopara.2011.01.004.
85. Grüring C, Spielmann T. 2012. Imaging of live malaria blood stage parasites. Methods Enzymol 506:81–92. https://doi.org/10.1016/B978-0-12-391856-7.00029-9.
86. Bachmann A, Scholz JAM, Janßen M, Klinkert M-Q, Tannich E, Bruchhaus I, Petter M. 2015. A comparative study of the localization and membrane topology of members of the RIFIN, STEVOR and PfMC-2TM protein families in Plasmodium falciparum-infected erythrocytes. Malar J 14:274. https://doi.org/10.1186/s12936-015-0784-2.
87. Collins CR, Hackett F, Strath M, Penzo M, Withers-Martinez C, Baker DA, Blackman MJ. 2013. Malaria parasite cGMP-dependent protein kinase regulates blood stage merozoite secretory organelle discharge and egress. PLoS Pathog 9:e1003344. https://doi.org/10.1371/journal.ppat.1003344.
88. Tonkin CJ, Van Dooren GG, Spurck TP, Struck NS, Good RT, Handman E, Cowman AF, McFadden GI. 2004. Localization of organellar proteins in Plasmodium falciparum using a novel set of transfection vectors and a new immunofluorescence fixation method. Mol Biochem Parasitol 137: 13–21. https://doi.org/10.1016/j.molbiopara.2004.05.009.
89. Blackman MJ, Whittle H, Holder AA. 1991. Processing of the Plasmodium falciparum major merozoite surface protein-1: identification of a 33-kilodalton secondary processing product which is shed prior to erythrocyte invasion. Mol Biochem Parasitol 49:35–44. https://doi.org/10.1016/0166-6851(91)90128-s.
90. Schindelin J, Arganda-Carreras I, Frise E, Kaynig V, Longair M, Pietzsch T, Preibisch S, Rueden C, Saalfeld S, Schmid B, Tinevez J-Y, White DJ, Hartenstein V, Eliceiri K, Tomancak P, Cardona A. 2012. Fiji: an open-source platform for biological-image analysis. Nat Methods 9:676–682. https://doi.org/10.1038/nmeth.2019.
91. Mesén-Ramírez P, Reinsch F, Blancke Soares A, Bergmann B, Ullrich AK, Tenzer S, Spielmann T. 2016. Stable translocation intermediates jam global protein export in Plasmodium falciparum parasites and link the PTEX component EXP2 with translocation activity. PLoS Pathog 12: e1005618. https://doi.org/10.1371/journal.ppat.1005618.
92. Struck NS, de Souza Dias S, Langer C, Marti M, Pearce JA, Cowman AF, Gilberger TW. 2005. Re-defining the Golgi complex in Plasmodium falciparum using the novel Golgi marker PfGRASP. J Cell Sci 118:5603–5613. https://doi.org/10.1242/jcs.02673.
93. Malleret B, Claser C, Ong ASM, Suwanarusk R, Sriprawat K, Howland SW, Russell B, Nosten F, Rénia L. 2011. A rapid and robust tri-color flow cytometry assay for monitoring malaria parasite development. Sci Rep 1: 118. https://doi.org/10.1038/srep00118.
94. Wichers JS, van Gelder C, Fuchs G, Ruge JM, Pietsch E, Ferreira JL, Safavi S, von Thien H, Burda P-C, Mesén-Ramirez P, Spielmann T, Strauss J, Gilberger T-W, Bachmann A. 2021. Characterization of apicomplexan amino acid transporters (ApiATs) in the malaria parasite Plasmodium falciparum. mSphere 6:e00743-21. https://doi.org/10.1128/mSphere.00743-21.
95. Galen SC, Borner J, Martinsen ES, Schaer J, Austin CC, West CJ, Perkins SL. 2018. The polyphyly of Plasmodium: comprehensive phylogenetic analyses

of the malaria parasites (order Haemosporida) reveal widespread taxonomic conflict. R Soc Open Sci 5:171780. https://doi.org/10.1098/rsos.171780.
96. Yu G, Smith DK, Zhu H, Guan Y, Lam TT-Y. 2017. ggtree: an R package for visualization and annotation of phylogenetic trees with their covariates and other associated data. Methods Ecol Evol 8:28–36. https://doi.org/10.1111/2041-210X.12628.
97. Yu G. 2020. Using ggtree to visualize data on tree-like structures. Curr Protoc Bioinform 69:e96. https://doi.org/10.1002/cpbi.96.
98. Katoh K, Standley DM. 2013. MAFFT multiple sequence alignment software version 7: improvements in performance and usability. Mol Biol Evol 30:772–780. https://doi.org/10.1093/molbev/mst010.
99. Madeira F, Park YM, Lee J, Buso N, Gur T, Madhusoodanan N, Basutkar P, Tivey ARN, Potter SC, Finn RD, Lopez R. 2019. The EMBL-EBI search and sequence analysis tools APIs in 2019. Nucleic Acids Res 47:W636–W641. https://doi.org/10.1093/nar/gkz268.
100. Davis MW, Jorgensen EM. 2022. ApE, A Plasmid Editor: a freely available DNA manipulation and visualization program. Front Bioinform 2:5. https://doi.org/10.3389/fbinf.2022.818619.
101. Lord SJ, Velle KB, Mullins RD, Fritz-Laylin LK. 2020. SuperPlots: communicating reproducibility and variability in cell biology. J Cell Biol 219:e202001064. https://doi.org/10.1083/jcb.202001064.
102. Tibúrcio M, Hitz E, Niederwieser I, Kelly G, Davies H, Doerig C, Billker O, Voss TS, Treeck M. 2021. A 39-amino-acid C-terminal truncation of GDV1 disrupts sexual commitment in Plasmodium falciparum. mSphere 6:e01093-20. https://doi.org/10.1128/mSphere.01093-20.
103. Eksi S, Morahan BJ, Haile Y, Furuya T, Jiang H, Ali O, Xu H, Kiattibutr K, Suri A, Czesny B, Adeyemo A, Myers TG, Sattabongkot J, Zhuan Su X, Williamson KC. 2012. Plasmodium falciparum gametocyte development 1 (Pfgdv1) and gametocytogenesis early gene identification and commitment to sexual development. PLoS Pathog 8:e1002964. https://doi.org/10.1371/journal.ppat.1002964.